(NASA-CR-120294) DESIGN AND FABRICATION OF PROTOTYPE SYSTEM FOR EARLY WARNING OF IMPENDING BEARING FAILURE (Mechanical Technology, Inc.) ~~84~~ 80 P HC $7.25

N74-28960

CSCL 13I G3/15 Unclas 43765

MTI . . . research and development division

MTI 74TR34

Design and Fabrication of Prototype System for Early Warning of Impending Bearing Failure

Prepared for

G. C. Marshall Space Flight Center
National Aeronautics and Space Administration
Huntsville, Alabama 35812

April, 1974

MECHANICAL TECHNOLOGY INCORPORATED
968 Albany-Shaker Road
Latham, New York 12110

NO. 74TR34

DATE: 4-74

TECHNICAL REPORT

DESIGN AND FABRICATION OF PROTOTYPE SYSTEM FOR EARLY WARNING OF IMPENDING BEARING FAILURE

John Meacher
H. Ming Chen
Author (s)

Approved

Approved

Prepared for

George C. Marshall Space Flight Center
National Aeronautics and Space Administration
Huntsville, Alabama 35812

Prepared under

NASA Contract NAS8-25706

MTI Project 0250-40077

MECHANICAL TECHNOLOGY INCORPORATED

968 ALBANY - SHAKER ROAD — LATHAM, NEW YORK — PHONE 785-2211

TABLE OF CONTENTS

FOREWORD

The work described in this report was performed by Mechanical Technology Incorporated, Latham, New York, under Contract NAS8-25706, awarded by the George C. Marshall Space Flight Center, National Aeronautics and Space Administration, Huntsville, Alabama.

The report presents a brief synopsis of the early parts of the program which were reported to NASA/MSFC in previously issued MTI technical reports:

1. MTI 71TR1 - "Design and Fabrication of Prototype System for Early Warning and Impending Bearing Failure", January, 1972
2. MTI 73TR33 - "Review of Mechanical Vibration Tests Conducted on Control Moment Gyros and Life Test Fixture", August, 1973

It also presents in detail the results of additional experimental work which was specified in contract modification No. 12, and which have not been previously reported to NASA/MSFC.

SYNOPSIS

A test program was conducted with the objective of developing a method and equipment for on-line monitoring of installed ball-bearings to detect deterioration or impending failure of these bearings. The program was aimed specifically at the spin-axis bearings of the Bendix ATM Control Moment Gyro (CMG). These were similar in internal geometry to Barden 107H angular contact ball bearings, 35 mm bore diameter.

Bearings were tested at speeds of 6000 rpm and 8000 rpm, thrust loads from 50 to 1000 lbs., with a wide range of lubrication conditions, with and without a simulated fatigue spall implanted on the inner-race ball track. An accelerometer (frequency response to 50 KHz) mounted on the outer-race housing was used and proved to be an effective primary sensor for a bearing health-monitoring system.

It was concluded that a bearing monitor system based on detection and analysis of modulations of a fault-indicating bearing resonance frequency can provide a low threshold of sensitivity. Very slight faults producing no detectable signal by conventional methods can be detected by such a system. Test results and observations leading to this conclusion were as follows.

1. The passage of each ball over a pit or fault in the race surface produced an impact. A structural resonance of one of the bearing components was excited to "ring" by these repetitive impacts. For the standard-race 107H bearing, this was apparently the third-mode resonance of the inner race, at a frequency of 28 KHz.

2. A faulted bearing produced bursts of 28 KHz signal at a rate equal to the ball-passing frequency for the inner race, giving the signal the appearance of amplitude modulation.

3. The raw signal from the faulted bearing contained no detectable component at inner-race ball-passing frequency. This frequency could be detected by spectrum analysis after the 28 KHz signal had been "demodulated" or envelope-detected.

4. The frequency of the fault-indicating signal was essentially unaffected by changes of load and speed. In the unfaulted bearing, the amplitude did not vary with load and increased slightly with speed.

5. The average amplitude at 28 KHz in a faulted bearing was from 12 to 50 times greater than in the unfaulted bearing.

6. Differences in ball-track surface condition of standard-race bearings could be inferred by comparing peak and average levels of the envelope-detected 24 KHz resonant frequency.

7. Long operating life caused increased amplitude at high frequency. However, this was of uniform amplitude characteristic of general wear and roughness, not the modulated amplitude expected from discrete faults.

Further conclusions resulting from the test program are as follows.

1. A "heavy-race" bearing designed specifically for the CMG application had different resonant frequencies. The dominant frequency produced by heavy-race bearings was dependent on thrust load, varying from 34 KHz to 58 KHz. The load-independent resonant frequency of the heavy-race bearing was 15 KHz.

2. Indications were seen that the fault-indicating resonance frequency of a bearing race will vary when different mounting or installation means are employed.

3. Evidence was encountered that nonuniform signal attenuation over the frequency-range of interest may result when an accelerometer must be installed on the exterior of large, complex structure wherein the monitored bearing is installed.

4. A qualitative indication of lubricant starvation was noted in that vibration amplitudes at all prominent frequencies increased notably when a minimal oil flow was interrupted.

A system to detect the presence of fatigue spalls, brinelling and general roughness of balls and races at a very low threshold level was successfully developed. Further development and expansion of the system is still required to detect and provide early warning of inadequate lubrication and ball-retainer distress.

I. INTRODUCTION

Rolling-element bearings have been in use for many years, and have proven to be reliable and long-lived when properly applied and installed. This excellent record of service, together with continued improvement in materials, design, and lubrication technology, have led to more and more stringent application requirements. These requirements include higher loads, higher rotational speeds, longer operating life, and, in some applications, restricted lubrication in high vacuum environments. These requirements are uniquely stringent for spin-axis bearings of gyroscopes aboard long-life space vehicles.

The space-vehicle gyroscope application has resulted in demands for very long life under conditions where only minimal lubrication can be provided, and servicing or re-lubrication cannot be performed. In addition, continued proper operation of the bearings is vital to the mission of the entire vehicle. Under these conditions, some accounting must be made for the possibility of failure of an individual bearing prior to mission completion, despite the excellent service record of rolling-element bearings as a group. One approach to this situation is to provide a back-up gyroscope aboard the vehicle with the intent of starting it and shutting down the primary unit if the bearings show signs of distress.

Implementation of this plan requires a device or system which can detect impending failure of a bearing, prior to the point where the bearing can no longer meet its design operating requirements. For many industrial applications, these requirements are rather loose, and admit relatively severe deterioration of a bearing from the initial "new" condition. Gyroscope applications, however, are more demanding and little degradation can occur before a faulty spin-axis bearing could jeopardize the function of the gyroscope. A fault-detection system with sensitivity meeting these demands was not available at the inception of the work reported herein. This work was aimed at developing such a system.

Objectives and Scope

A test program was conducted with the objective of developing a method and equipment for on-line monitoring of installed ball-bearings to detect deterioration or impending failure of these bearings.

The program was aimed specifically at the spin-axis bearings of the Bendix ATM Control Moment Gyro (CMG) installed on the NASA Sky Lab Vehicle. This was stated to be similar in internal geometry to a Barden 107H angular contact ball bearing, 35 mm bore diameter.

Target criteria for the monitoring sensor and system were:

1. Sensor installation must not restrict normal operation of the bearing;
2. The sensor and system should produce positive indications of a bearing fault or deterioration well before the bearing ceases to perform its design function;
3. The system output or indicating signal should vary with the state of bearing deterioration to permit predictions of remaining operational life;
4. The sensor and system should ideally be unaffected by bearing operating variables such as load, speed, temperature, etc.

It was desired that the system recognize and indicate the following specific conditions:

1. Beginning of fatigue failure;
2. Brinelling of bearing surfaces;
3. Flooding or starving of lubricant;
4. Change in the lubrication process from an elasto-hydrodynamic film to a condition of intermittent contact at surface asperities.

II. SUMMARY, CONCLUSIONS AND RECOMMENDATIONS

A test program was conducted with the objective of developing a method and equipment for on-line monitoring of installed ball-bearings to detect deterioration or impending failure of these bearings. The program was aimed specifically at the spin-axis bearings of the Bendix ATM Control Moment Gyro (CMG) installed on the NASA Sky Lab vehicle. These were essentially Barden 107H angular contact ball bearings, 35 mm bore diameter.

Three standard class 7, 107H bearings were tested at speeds of 6000 rpm and 8000 rpm, thrust loads from 50 to 1000 lbs., with a wide range of lubrication conditions. One of the test bearings had a simulated fatigue spall implanted on the inner-race ball track. During tests, data signals were recorded from a wide diversity of sensors. Analyses of these data revealed that ultrasonic vibrations were the only means by which the implanted fault could be reliably detected. A high-frequency response accelerometer mounted on the outer-race housing provided the most informative signal of all sensors used. Results from these tests were as follows.

1. The 107H bearing produced an ultrasonic vibration frequency of 28 KHz which was an effective fault indicator.
2. The frequency of the fault-indicating signal remained relatively constant when load and speed were changed. In the unfaulted bearing, the amplitude did not vary with load and increased only slightly with speed.
3. The average amplitude at 28 KHz in a faulted bearing was from 12 to 50 times greater than in the unfaulted bearing.
4. The faulted bearing produced bursts of 28 KHz signal at a rate equal to the ball-passing frequency for the inner race, giving the signal the appearance of amplitude modulation.
5. The raw signal from the faulted bearing contained no detectable component at inner-race ball-passing frequency. This frequency could be detected by spectrum analysis only after the 28 KHz signal had been "demodulated" or envelope-detected.
6. It was concluded that the passage of each ball over the implanted pit or fault produced an impact. The 28 KHz was a structural resonance of one of the bearing components which was excited to "ring" by these repetitive impacts.

7. It was also concluded that a bearing monitor system based on detection and analysis of modulations of the fault-indicating resonance frequency would provide a very low threshold of sensitivity. Very slight faults producing no detectable raw signal at ball-pass frequency can be readily detected by such a system.

A Bearing Fault Detector based on the above concept and the 28 KHz frequency was built and delivered to NASA for use with the 107H bearing. Field measurements of vibration were made on 6 CMG flight units, 2 Inner Gimbal Rotor Assemblies, and 6 Life Test Fixtures. The data were used to establish a qualitative ranking of these units, which is included in Appendix B of this report. Further conclusions from these tests were:

8. Long operating life caused an increased vibration amplitude at high frequency. However, it was a uniform amplitude, characteristic of general wear and roughness, and not the modulated amplitude expected from discrete faults.

9. Some of the CMG bearings exhibited a "squeal" phenomenon associated with the phenolic ball retainer. The squeal frequencies of 900 Hz and 3100 Hz were believed to be symptoms of retainer distress.

A series of resonance tests were made on the balls and races of the 107H bearing in an attempt to identify the source of the 28 KHz frequency. Conclusions from these tests were:

10. The third-mode resonance of the inner race was the most probable source of the 28 KHz.

11. The ball-contact resonance was not the source of 28 KHz;ball-contact resonant frequency increased markedly with load, from 30 KHz to 37 KHz.

12. Both inner and outer races exhibited several other resonant frequencies in the range from 13 KHz to 47 KHz.

13. Resonant vibration of the inner race was apparently transmitted through the balls, the outer race, and the outer-race housing to the sensing accelerometer during tests on the rotating spindle.

Bearings were mounted on a different test spindle ("endurance rig") and run at 4000 rpm under high thrust load with intent to produce fatigue failure, and

observe the change of 28 KHz vibration during the progress of the failure. Results and conclusions were as follows:

14. The fault-indicating frequency of the 107H bearing shifted from 28KHz to 24 KHz when installed on the "endurance" test rig.

15. Evaluation of the monitoring technique and its ability to provide early warning of failure was inconclusive due to the shift of fault-indicating frequency. There is partial evidence that the technique would have succeeded had 24 KHz been monitored.

16. The more probable failure mode for the 107H CMG bearing is ball-retainer failure due to inadequate lubrication. Fatigue failure producing discrete spalls or faults is less likely under marginal lubrication conditions.

Further tests were performed in the endurance rig to identify the fault-indicating frequency and signal levels of several bearings, including the special "heavy-race" bearings built specifically for the CMG. Qualitative ranking of these bearings was formulated and included herein, based on data from these endurance-rig tests. The additional endurance-rig tests produced the following results and conclusions.

17. The fault-indicating resonant frequency of the standard-race bearing definitely shifted from 28 KHz to 24 KHz when installed in the endurance rig. The shift was apparently caused by some aspect of the inner-race mounting on the test-rig spindle.

18. Differences in ball-track surface condition of standard-race bearings could be inferred by comparing peak and average levels of the envelope-detected 24 KHz resonant frequency.

19. The dominant frequency produced by heavy-race bearings on the endurance rig was strongly dependent on thrust load, varying from 34 KHz at 50 lb. load up to 58 KHz at 1000 lb. load.

20. The load-independent resonant frequency of the heavy-race bearing on the endurance rig was 15 KHz.

Final tests consisted of running four heavy-race bearings in a Life Test Fixture, and comparing the data with that from the same four bearings run on the endurance rig. Results and conclusions were as follows:

21. The massive bearing-housing structure of the LTF acted as a high-pass filter. This caused severe attenuation of the load-independent 15 KHz fault-indicating frequency of the heavy-race bearing compared to endurance-rig results. The load-dependent component (34 KHz to 58 KHz) was attenuated much less.

Recommendations

The objectives of the program have been partially achieved; a means of detecting surface defects such as fatigue spalls or Brinell marks was developed. A course of action to achieve the remaining objectives is discussed below.

Attention must be concentrated on the mode of bearing failure in which the ball retainer is apparently the key element. Field measurements on CMG's conducted during this program indicate that the ball retainer encounters distress; the test-to-failure resulted in a large increase in bearing torque apparently due to retainer failure. This increase in torque apparently has been the prevalent failure mode plaguing the CMG units aboard the Skylab. The tests reported herein indicate that retainer failure is caused by or related to marginal lubricant supply. Therefore, the following work is recommended.

1. Determine which type of bearing is most widely used in CMG units, the standard-race or the heavy-race bearing. Confine further testing to the more prevalent type of bearing.

2. Conduct further operational bearing tests to accurately define the nature of the change in vibration behavior which occurs during the course of retainer deterioration. The number of variables must be minimized to insure positive achievement within the constraints of a realistic budget and schedule. Tests should be run at constant load and speed identical to those of the CMG application. (Thrust load is probably not a determining variable affecting retainer failure, whereas speed and the consequent rubbing velocities and inertial forces within the bearing undoubtedly are determining factors in retainer failure.) The single operating variable should be the lubrication condition.

3. A definition of "bearing failure" must be formulated: a key performance variable must be identified and a quantitative threshold of acceptance established which represents the boundary of a "failure" condition. For the CMG bearing, this must certainly be bearing torque. Consequently, this variable should be measured during the recommended tests. Changes in vibration behavior must then be correlated with changes in torque. When this is accomplished, a "yardstick" of bearing acceptability and/or future life can be defined in terms of the measured vibration behavior. A diagnostic system to implement this measuring scheme can then be fabricated.

III. INITIAL ROTATING SPINDLE TESTS

The work reported herein evolved through four phases:

- Phase I - first rotating spindle tests and construction of a prototype failure-detection and diagnostic system
- Phase II - field tests of gyroscope units
- Phase III - investigation of resonances of bearing races and balls
- Phase IV - continued tests and development of diagnostic technique

The first tests were run on a spindle previously installed at MTI as part of a Hybrid Boost Bearing test rig. This spindle could be operated at speeds equal to that of the gyroscope wheel, and under thrust loads greater than that experienced by the gyroscope bearings. Actual gyroscope bearings were not immediately available for testing, so the closest commercial equivalent bearings were obtained for these first tests. These were Barden 107H bearings, ABEC grade 7. The characteristics of this test bearing are tabulated in Appendix A-1.

No effort was made during these first tests to produce actual fatigue failure. It was assumed that the onset of fatigue failure would be embodied in a first discrete fatigue spall or pit. This could be simulated by implanting a discontinuity in the surface of the ball track of the inner race, where fatigue failure would probably first occur. This would also approximate a single Brinell mark.

Test Conditions

Three new, standard 107H bearings were tested sequentially on a laboratory test spindle under varied operating conditions. Appendix A-2 is an assembly drawing of the spindle, and Appendix A-3 is a photograph of the spindle. One of the 107H bearings was tested both before and after a simulated fatigue spall was implanted on the ball track of the inner race. Appendix A-4 shows the nature of the implanted fault.

The test conditions consisted of combinations of the following values:

Radial Load lbs.	Thrust Load lbs.	Shaft rpm	Lubrication Conditions
	50	6000	(Esso 2389 Turbo Oil, MIL-L-7808)
15	250	8000	a. full flow (0.1 gpm)
(constant)	1000		b. no flow c. dry, washed in solvent

Measured Variables and Sensors

In order to identify sensors capable of detecting bearing condition, all of the measurement sensors listed below were employed during all tests.

	Variable	Frequency Range	Sensor	Location
1.	Vibration	to 50 KHz	Wilcoxon acceler.	outer-race housing
2.	Ultrasonic energy	36 KHz to 44 KHz	Delcon 4950A translator	outer race
3.	Temperature	--	Thermocouple	outer race, oil inlet and outlet
4.	Shaft displacement	to 5 KHz	Eddy-current proximity probe	shaft, radial
5.	Torque	to 20 KHz	Strain gages	supporting arms for outer-race housing
6.	Strain	to 20 KHz	Strain gages and PZT-4 crystal	outer race, circumferential
7.	Vibration	to 15 KHz	Accelerometer	outer-race housing
8.	Airborne noise	to 20 KHz	Microphone	6 inches from test bearing

The success or applicability of each of these sensors in detecting the presence of the simulated fatigue fault or other required conditions are stated below.

1. Accelerometer, "high" frequency Wilcoxon - maximum definition of bearing condition and discrimination of fatigue fault.
2. Ultrasonic translator - output increased by factor of 16 from good to faulted bearing; inadequate for specific diagnosis of fault.

3. Temperature - the only sensor which could detect presence or lack of oil flow; no other useful data
4. Proximity probe - no useful data
5. Torque - no useful data
6. Strain gage and PZT-4 crystal - no useful data
7. Accelerometer, "low" frequency - no useful data
8. Microphone - no useful data

Results and Conclusions

The frequency spectrum of the Wilcoxon accelerometer signal contained dominant components at about 28 KHz and at 50 KHz to 55 KHz. The presence of the implanted fatigue fault was clearly indicated by changes in the 28 KHz component. The behavior of the signal under varying conditions is summarized below.

1. The frequency of the fault-indicating component always occurred within a narrow range from 27.5 KHz to 31 KHz and did not shift consistently with speed or load.
2. In an unfaulted bearing, the amplitude of this frequency component did not vary significantly with load, and increased only slightly with speed. This is demonstrated by the frequency spectrum plots of Figure 1.
3. The amplitude in a faulted bearing was from 12 to 50 times greater than that in the unfaulted bearing. The amplitude increased significantly with load in the faulted bearing. This is shown by the spectrum plots of Figure 2.
4. The raw signal from the faulted bearing contained no detectable amplitude at the inner-race ball-passing frequency (corresponding to the impacting of individual balls on the single fault implanted on the inner race).
5. The inner-race ball-passing frequency was clearly evident in the faulted-bearing signal as a modulation of the 28 KHz "carrier" frequency. This could be identified by spectrum analysis only after the 28 KHz signal had been "demodulated" or envelope-detected. This fact is illustrated by the low-frequency spectrum plots of Figure 3.

Bearing Fault Detector

Based on the findings stated above, a Bearing Fault Detector (shown in Figure 4) was built and delivered to NASA. This device was designed to receive the output from an accelerometer and charge amplifier, which was band-pass filtered at a center frequency of 28.5 KHz. The shape of the filter characteristic is shown in Appendix A-5. The filtered carrier signal was then envelope-detected, and the resultant signal was directed through a tuneable band-pass filter. This allowed analysis to determine the modulating frequency and thereby identify a fault on the inner race, outer race, or on a ball. A fault-indicating light was illuminated when both the average amplitude at 28 KHz and the modulation amplitude exceeded limit values. A schematic of the Fault Detector is shown in Figure 5.

This concluded the initial phase of the contract, and the work was summarized in Report MTI 71TR1, January, 1972.

IV. FIELD TESTS OF CMG, IGRA, AND LTF UNITS

Phase II consisted of measuring and analyzing vibration and airborne noise on 6 CMG flight units, 2 engineering Inner Gimbal Rotor Assemblies (IGRA) and 6 Life Test Fixtures (LFT). The test measurements were taken during the period from January, 1971, through July, 1972, at three locations:

1. Marshall Space Flight Center
2. Wyle Laboratories, Huntsville, Alabama
3. Bendix Corporation, Teterboro, New Jersey

Measuring Sensors

The following measuring sensors were employed during these tests:

1. High-frequency accelerometer - Bruel and Kjaer Model 4344 (newly available, to replace the previously used Wilcoxon sensor);
2. Low-frequency accelerometers - for measuring vibration at rotational and twice-rotational frequencies;
3. Microphone - inserted inside the port in the CMG cover.

Results and Conclusions

Two significant facts emerged from these tests and the resulting data.

1. Those gyro bearings which had experienced many hours of operation did show relatively higher vibration amplitudes in the high frequency range. However, it was a uniform high amplitude, characteristic of general wear, and not the modulated amplitude expected from discrete faults.
2. Deterioration of the phenolic ball retainer appeared to be a more common failure mode for the CMG bearings. Symptoms of this failure were noted in several of the units tested. The symptoms were significant responses at 900 Hz and 3100 Hz in the vibration spectrum and in the audible airborne-noise spectrum. These symptoms could not be detected by the Bearing Fault Detector, which responded only to 28 KHz.

A qualitative ranking of performance was established for all of the tested units, based on the amplitudes of the following components of the measured noise and vibration data.

1. Rotational frequency - rotor balance;
2. Twice rotational frequency - bearing misalignment, possibly due to gimbal supports;
3. 900 Hz and 3100 Hz - ball-retainer condition;
4. 20 KHz to 30 KHz - condition of ball-track surfaces.

The actual ranking of tested units is presented in Appendix B. The testing and analysis performed during Phase II was summarized in Report MTI 73TR33, August, 1973.

V. BALL AND RACE RESONANCE TESTS

The work of Phase III consisted of laboratory tests aimed at identifying the source of the 28 KHz fault-indicating signal observed during Phase I bearing tests. It had been surmised during Phase I that this frequency was related to the mass of a ball and the stiffness of the supporting contact between the ball and races. A test program was devised to examine the validity of this premise.

Resonance Test Fixture

A ball was to be clamped between two surfaces under a controlled compressive force, and subjected to vibratory excitation by a piezoelectric crystal. The excitation frequency would be swept through a range up to 100 KHz. The relative response amplitude would be measured with a second piezoelectric crystal. The exciting and measuring crystals were interposed between the ball and the steel members through which compression load was applied. The load was measured with a strain-gage load cell. This test fixture is shown assembled in Figure 6, and disassembled in Figure 7. After testing the ball for resonant frequencies, the inner and outer races of the 107H bearing were tested in a similar manner, as indicated in Figure 8.

The intent of these tests was two-fold:

1. to identify resonant frequencies inherent to the specific bearing components;
2. to determine whether or not these frequencies varied with bearing load.

The load imposed on the ball by the test fixture was very similar to that which the ball experiences in the assembled bearing. However, the diametral load imposed on the races by the fixture was not truly representative of the load conditions which arise from a thrust load in an assembled bearing. The frequency-load relationships indicated by the tests on the races are therefore not conclusively definitive.

Results

The results from these resonance tests are shown in Figure 9 as plots of resonant frequency versus load. The resonant frequency of the ball increased with load from 30 KHz up to 37 KHz. This did not agree with the load-invariant 28 KHz frequency observed during bearing tests. It was concluded that the fault-indicating 28 KHz was not due to ball resonance. Several resonances were identified in both the inner and outer races, as shown in Figures 10 and 11. The third mode of the inner race and the fifth mode of the outer race both occurred between 26 KHz and 27 KHz and appeared to be possible sources of the 28 KHz signal of interest.

The race resonances were further explored by a method illustrated in Figures 10 and 11. The bearing outer race was mounted in the housing of the bearing test rig, as shown in Figure 10. One accelerometer was mounted on the I.D. of the race as a "driver" and excited with a signal generator. A second accelerometer was mounted on the O.D. of the housing as a sensor. The driver frequency was then swept through the range of interest, and the relative response amplitude at the sensor was recorded. A similar procedure was performed on the inner race, when mounted on the bearing-test-rig fixture shown in Figure 8. An assembled bearing was also tested in this manner. The results are shown in Figure 12.

Conclusions

It is apparent in the data of Figure 12 that the resonances of the separate races are somewhat altered when assembled in the bearing. This introduced some confusion in the results, and positive conclusions could not be drawn. However, it was tentatively concluded that the 28 KHz fault-indicating frequency was a resonance of the inner race. No explanation could be conceived as to why that particular resonant frequency had dominated the vibration spectrum of the bearing when operated under load on the test spindle.

The results of Phase III work can be summarized in the following conclusions.

1. The .310 inch diameter ball of the 107H bearing has a contact resonance which varies in frequency from 30 KHz to 37 KHz, depending on the compressive load.

2. The ball-contact resonance was not the source of the fault-indicating 28 KHz signal observed during rotating bearing tests.

3. The outer race of the 107H standard bearing exhibited several resonant frequencies in the range from 13 KHz to 45 KHz, which varied only slightly with load, but none of which appeared to be the source of the 28 KHz in the assembled bearing.

4. The inner race also exhibited several resonances, the third mode resonance appearing to be the most likely source of the 28 KHz noted during rotating tests.

5. Resonant vibration of the inner race was apparently transmitted through the balls, the outer race, and the outer-race housing to the sensing accelerometer during tests on the rotating spindle.

VI. TESTS-TO-FAILURE IN ENDURANCE RIG

Phase IV included three activities listed below.

1. Rotating tests-to-failure of three standard-race 107H bearings, sequentially mounted on an "endurance" rig;
2. Rotating tests of four standard-race bearings and four "heavy-race" bearings in the endurance rig, to identify the fault-indicating frequency and signal level at these frequencies;
3. Rotating tests in a Bendix LTF (Life Test Fixture) of four heavy-race bearings, and comparison with similar tests in the "endurance" rig, to assess signal attenuation caused by LTF structure.

Endurance Test Rig

The tests-to-failure were run on the "endurance" rig, which was a different test spindle than that used for the initial Phase I tests. The spindle is shown schematically in Figure 13, and Figure 14 is a close-up photo of the active spindle. The test instrumentation for the endurance tests-to-failure is shown in Figure 15. The rig contained three spindles, only one of which was used. The spindle was limited to a maximum speed of 5000 rpm, and the tests were run at about 4000 rpm.

Instrumentation

A Bruel and Kjaer Model 4344 miniature accelerometer was stud-mounted to the outer-race housing of the test bearing, as shown in Figures 13 and 14. The output signal was routed to the following processors:

Processor	
Peak Meter	Peak amplitude of raw signal
28 KHz band-pass filter to peak meter and rms meter	Peak and average amplitudes of filtered signal
Envelope detector	Peak amplitude and DC level of envelope-detected 28 KHz signal
Hi-pass filter (200 Hz cutoff)	Peak and average amplitude of envelope-detected signal, excluding components below 200 Hz (primarily rotational)

All peak meters and average meters used for the test produced DC output signals proportional to the measured AC level. These signals were continuously recorded on a Honeywell multipoint strip-chart recorder.

First Test: No Failure

The test bearings were new, Class 9, Barden 107H bearings. The first bearing was initially lubricated with several drops of SAE 30 oil. After running several hours with no additional oil, the bearing became noisy. An air-oil mist lubricator was then devised and installed, using Turbo-S-Oil No. 15. Oil flow was adjusted to suppress bearing noise. The test was then run continuously at 4000 rpm as follows:

Duration	Thrust Load	Results
750 hrs.	800 lbs.	No detectable change
500 hrs.	1100 lbs.	No detectable change

1250 hrs., total running time--test terminated.

A review of frequency-spectrum plots of the raw signal made periodically during the course of this test revealed a gradual and slight increase of a component at 25 KHz. It appeared that more severe operating conditions were required to produce failure within the time available.

Second Test

The second test bearing was installed and run at 4000 rpm, 1100 lb. load as follows:

Duration	Lubrication	Results
93 hrs.	Drop-type oiler, 3 drops/minute, SAE 30 oil	No change
7 hrs.	no oil added	a. bearing torque increased and stalled the spindle drive; b. slight roughening of balls and races; c. accumulation of wear debris from ball retainer on outer race; d. no warning by increased vibration amplitudes.

Duration	Lubrication	Results
(test continued; bearing not cleaned or oiled)		
6 hrs.	No oil added	a. vibration amplitudes were significantly higher at start of this period; b. bearing torque increased to stall the spindle at end of period; test terminated; c. rise in temperature of outer race; d. retainer wear debris on both races; e. no discrete pits or spalls, but balls and ball-tracks show general roughening.

Conclusions from Monitored Data

Plots of accelerometer signal levels through the course of this test are presented in Figure 16. Two conclusions can be drawn from the plots of Figure 16.

1. The raw signal total peak-to-peak amplitude displayed the same characteristic history and was equally as informative as any of the band-pass filtered or envelope-detected signals.
2. None of the recorded signals provided an identifiable "early warning" of the "seizures" which occurred during this test.

Third Test

A third test bearing was installed on the spindle directly from its sealed package. No lubrication was added. This bearing "seized" almost immediately. Examination revealed stripes of phenolic retainer material on balls and races.

Discussion of Results of Second Test

Frequency spectrum plots of the raw accelerometer signal were made periodically during the test-to-failure of bearing S/N 6. Four of these are shown in Figure 17. It is apparent from these plots that the fault-indicating frequency during this test was between 23 KHz and 25 KHz, and not at 28 KHz. The shape of the 28 KHz filter was such that a 24 KHz signal would be attenuated to about one-fifth of its initial amplitude. Consequently, the results of this test were inconclusive, so far as providing data for evaluating the condition-monitoring technique. A

review of all the frequency spectrum plots taken during the test does lead to the tentative conclusion that a more rapid rise in amplitude at 24 KHz did occur near the end of the test. This might have provided an "early warning" of failure if this frequency had been continuously monitored. The shift of the fault-indicating frequency during the tests-to-failure will be further discussed in the next section.

Conclusions from Tests-to-Failure

In summary, the following conclusions were drawn from the results of the tests-to-failure of the 107H CMG ball bearing.

1. The fault-indicating frequency of the 107H bearing was shifted from 28 KHz to 24 KHz when installed on the "endurance" test rig.
2. Evaluation of the condition monitoring technique and its ability to provide early warning of failure was inconclusive, since the wrong frequency was monitored. There is partial evidence that the technique would have succeeded if 24 KHz had been monitored.
3. The more probable failure mode for the 107H CMG bearing is ball-retainer failure due to inadequate lubrication. This will cause wear of the phenolic retainer, build-up of phenolic debris in the ball tracks, excessive bearing torque, and general roughening of ball and race surfaces. Fatigue failure producing discrete spalls or faults will probably not occur unless very long operation occurs under conditions of good lubrication.

VII. FURTHER TESTS IN THE "ENDURANCE" RIG

Four samples of the 107H "standard-race" bearing were tested on the endurance rig to identify the fault-indicating frequency. In addition, four special "heavy-race" bearings were similarly tested.

Test Procedure

The test procedure was as follows.

1. Mount the accelerometer (B & K 4344) radially on the bearing outer-race adaptor, with a mounting stud.
2. Lubricate the test bearing with several drops of TURBO-S-OIL No. 15. Apply thrust load to the bearing and run the spindle to the desired speed (4000 rpm or 5000 rpm). Wait for warm-up and steady operation.
3. Using the transient recorder and real-time analyzer, plot the frequency spectrum of the raw signal. The spectrum will indicate the predominant fault generated resonance frequency.
4. Measure the raw signal amplitude with a peak meter.
5. Set the center frequency of a band-pass filter at the fault-generated resonance frequency as indicated by the spectrum. Measure the filtered output peak value and average value.
6. Feed the filtered high frequency signal into an envelope detector. Use the real-time analyzer to plot the frequency spectrum of the envelope signal. Measure the peak value and DC level of the envelope.
7. Pass the envelope signal through a low frequency band-pass filter. Set the center frequency at the precalculated ball pass frequency. Measure the filtered output peak value and average value.

The installation for these tests was identical to that for the tests-to-failure, shown in Figure 14.

Tests of Standard-Race Bearings

The signal levels recorded during these tests of standard-race bearings are presented in Tables I thoough IV. Frequency spectrum plots of the raw and envelope-detected signals from bearing serial number 3 are shown in Figure 18. This was the identical faulted bearing which was used during Phase I tests and which produced the 28 KHz fault-indicating frequency. It is apparent in Figure 18 that the load-independent, fault-indicating frequency was 24 KHz. A component at 36 KHz was prominent at 50 lb. load, but this frequency appeared to shift upward as the load was increased. Frequency spectrum plots for bearings S/N 4, S/N 9, and S/N 10 were similar in frequency content, though much lower in amplitude since they were not faulted as was S/N 3.

Shift of Fault-Indicating Frequency from 28 KHz to 24 KHz

Resonance tests were run on the outer-race housing used on the endurance rig in an effort to identify the cause or source of the new 24 KHz resonant frequency. The bearing outer race installed in the endurance-rig housing did not display a resonant frequency in the range 23 KHz to 26 KHz. Bearing S/N 3 was operated on another small test spindle and again produced 28 KHz, but not 24 KHz.

It can be noted in Table I that the amplitude of the 24 KHz component decreased consistently with increasing thrust load. On the Phase I test spindle, the 28 KHz amplitude from a faulted bearing increased with load. There was one aspect of the endurance rig which could account for this different behavior; the inner-race mounting adapter was secured to the spindle on a taper, as shown in Figure 13. Increased thrust load therefore tended to tighten the fit of the adapter in the inner race and onto the spindle, also. The Phase I test spindle had no taper fits, so that radial fits were unaffected by thrust load. It was therefore concluded that some aspect of the inner-race mounting on the endurance-rig spindle shifted the inner-race resonance from 28 KHz to 24 KHz, and caused the different behavior under increasing thrust load.

Ranking of Standard-Race Bearings

The data from Tables I through IV were used to rank the condition of the four standard-race bearings as follows.

1.	S/N 10 -- best	slight roughness, trace indication of discrete faults
2.	S/N 9 -- slight margin below S/N 10	same surface characteristic as S/N 10
3.	S/N 4 -- poorer	general roughness about the same as S/N's 9 and 10; indication of discrete faults definitely stronger
4.	S/N 3 -- bad	dominant indication of discrete fault; (this was the faulted test bearing)

The above statements concerning surface condition of the test bearings are based solely on the peak, average, and DC values given in Tables I through IV. Generally speaking, for diagnostic purposes, the peak and average values of a filtered signal at the resonance frequency are adequate to discriminate a bad bearing from a good one. High peak value is an indication of discrete fatigue spalls or large-particle retainer debris on the contact surfaces. High average value is an indication of distributed roughness of contact surfaces due to general wear or small-size debris accumulation. The peak and DC levels of the envelope-detected signal are redundant information. The filtered envelope peak value at different ball-pass frequencies can be used to identify the location of faults in the bearing. As mentioned before, for the 107 bearings, the ball-pass frequency for a discrete spall on the inner race is 8.7 times inner-race rotational speed. It is 6 times inner-race rotational frequency if the fault is on a ball; it is 6.3 times rotational frequency if the fault is on the outer race.

Heavy-Race Bearings

The CMG was designed to use a special version of the 107H bearing which had larger inner and outer races, and is designated here as the "heavy-race" bearing. Section drawings of the standard and heavy-race configurations are shown in Figure 19 for comparison. It is apparent therein that the race structures are sufficiently different that the resonant behavior and frequencies would be dissimilar.

Two heavy-race bearings were tested on the endurance rig to identify the fault-indicating frequency; bearing S/N 3 was deliberately faulted on the inner race in a similar fashion as was the standard bearing of Phase I. The test procedure was identical to that employed for standard bearings. The recorded signal

levels are tabulated in Tables V through VIII. Two additional heavy-race bearings were removed from Life Test Fixture unit number 5 and tested on the endurance rig as part of the LTF test series. Results of these tests are presented in the next section.

Fault-Indicating Frequencies of Heavy-Race Bearings

Frequency spectrum plots of the raw signal from the faulted bearing (S/N 3) and the used bearing (S/N 4) at speeds of 4000 rpm and 5000 rpm at five different loads are shown in Figure 20.

Three resonant peaks are prominent in these plots:

a. 7 KHz - considered too low for diagnostic use, since it is within the range of much machinery noise;
b. 14 - 16 KHz - frequency varies slightly with thrust load, amplitude increases with speed; appears to be the best fault indicator;
c. 35 KHz - frequency increases significantly with thrust load, goes up to 58 KHz at 1000 lb. load.

A band-pass filter and the envelope-detector were utilized to assess the modulation of these frequencies. Frequency spectrum plots of the envelope-detected signal at 4000 rpm at 15 ± 1 KHz and at the load-dependent frequency (35 KHz to 58 KHz) are shown in Figure 21. The inner-race ball-pass frequency is clearly evident in the envelope-detected 15 KHz component from the faulted bearing, and is not evident in the comparable signal from the "used" bearing. Modulation of the 35 to 58 KHz frequency apparently becomes stronger with increasing thrust load for the faulted bearing, but is relatively weak in the used bearing.

Tables V and VI are the recorded signal levels from the faulted and used bearings, based on the 15 KHz fault-indicating frequency. Tables VII and VIII are similar data based on the load-dependent frequency, wherein the filter center frequency was shifted with load to follow this frequency. In both sets of data the faulted bearing produces much higher levels than the used bearing in all types of signal. The ratios of peak-to-average signal are roughly comparable for both the used and faulted bearings. This leads to the conclusion that whatever faults exist in the used bearing have the nature of discrete faults.

Conclusions

The additional tests in the endurance rig lead to the following conclusions.

1. The fault-indicating resonant frequency of the standard-race bearing definitely shifts from 28 KHz to 24 KHz when installed in this rig, since four different bearings gave similar results.
2. The shift in frequency is apparently produced by some aspect of the inner-race mounting on the test-rig spindle.
3. Differences in ball-track surface condition of standard-race bearings can be inferred by comparing peak and avearge levels of the envelope-detected 24 KHz resonant frequency.
4. The dominant frequency produced by heavy-race bearings on the endurance rig was strongly dependent on thrust load, varying from 34 KHz at 50 lb. load up to 58 KHz at 1000 lb. load.
5. The load-independent resonant frequency of the heavy-race bearing on the endurance rig was 15 KHz. The amplitude at this frequency was an effective indicator of an implanted discrete fault.

VIII. TESTS IN THE LIFE-TEST FIXTURE

The final tests of the program were run on a Bendix CMG Life Test Fixture, P/N 2123570, provided by NASA. This LTF unit incorporates the CMG bearings, a shaft, and spin motor in an enclosure which can be evacuated for high-speed operation. The bearings are mounted in six-sided aluminum plates, 2 inches thick, 14 inches maximum length. An accelerometer for sensing bearing vibration could only be mounted on the outer edge of these large plates. The vibration would therefore have to traverse several interfaces at mounting fits and then the radial length of the heavy mounting plates. It was anticipated that this signal transmission path would impose significant impedance and cause some attenuation. It was proposed that these effects be assessed by comparative tests of identical bearings in the LTF and in the endurance rig.

Test Procedure

The LTF incorporated heavy-race bearings S/N 003 and S/N 012 when received at MTI. Provision for mounting the sensing accelerometer was made on the edge surface of the bearing housing plate at each end of the rig. Small aluminum plates 3/4 inch square by 1/4 inch thick were drilled and tapped for the accelerometer mounting stud. These were then bonded to the LTF bearing housing plate at the desired location with cyano-acrylate adhesive. The accelerometer could then be stud-mounted on these plates, which were left in place throughout all LTF tests, so that no variability was introduced by re-cementing the plates.

The LTF was run at speeds of 4000 rpm and 9100 rpm. This provided data for comparison with endurance-rig tests at 4000 rpm, and for comparison with data from CMG units, which are intended to run at about 9000 rpm. The spin motor was energized with a CML MACARR Model T500B three-phase variable frequency converter. The LTF housing was evacuated during test runs to reduce windage losses.

After data were taken from the LTF with the original bearings (S/N 003 and S/N 012), these bearings were removed and replaced with heavy-race bearings S/N 3 and S/N 4, which had previously been tested on the endurance rig. The original LTF heavy-race bearings were subsequently tested on the endurance rig.

Results

Frequency spectrum plots of the raw signal from one of the original bearings (S/N 003) of the LTF are shown in Figure 22, for operation in the LTF and in the endurance rig. It is apparent from these plots that the strong resonances below 20 KHz in the endurance rig are very greatly attenuated in the LTF. The resonance between 32 KHz and 36 KHz becomes the dominant frequency in the LTF by a wide margin. It appeared that the signal transmission path in the LTF structure acted as a high-pass filter, and selectively attenuated frequencies below 20 KHz.

Similar frequency spectrum plots for the faulted bearing (S/N 3) are shown in Figure 23. The same apparent high-pass filtering phenomenon is evident therein.

Table IX presents a comparison of amplitudes of signals from endurance-rig and LTF tests of four heavy-race bearings at a speed of 4000 rpm. These include the two original LTF bearings (S/N 003 and S/N 012), plus the faulted and used alternates (S/N 3 and S/N 4). It is clearly evident from this tabulation that the signal is attenuated in the LTF, except for the faulted bearing. This exception is an anomaly that could not be explained.

Table X presents similar data for all four heavy-race bearings tested in the LTF at 9100 rpm. Comparison with Table IX data for LTF tests indicates that all amplitudes increase with speed. The data of Table X can also be used to rank the heavy-race bearings in the same manner that standard-race bearings were ranked in the previous section.

1. S/N 012 best condition (from "side 2" of the LTF)
2. S/N 4 slightly poorer (the "used" alternate bearing)
3. S/N 003 notably poorer than 012 (from "side 1" of the LTF)
4. S/N 3 poorest (faulted with similated fatigue spall)

The same ranking could be inferred from the raw signal, the filtered signal, the envelope-detected signal or the ball-pass frequency component of the envelope-detected signal. It might be concluded from this fact that filtering and envelope detection were unnecessary signal processing. However, in many monitoring situations, other machine components might be creating large-

amplitude signals at several frequencies. Filtering to exclude all but a preferred frequency would certainly be necessary. If unrelated components produced frequencies within the pass-band of the filter, modulation on the envelope-detected signal would allow positive identification of that vibration component and amplitude contributed by the bearing.

LIST OF TABLES

Speed RPM	Thrust Load (Lbs)	Accel. Raw Signal (Volts)	Filtered Signal at 25 KH_z		Envelope Detected Signal		Filtered Envelope Signal at Inner-Race Ball-Pass Freq.		Charge Amplifier Setting (MV/G)
			Peak (Volts)	Ave (RMS Volts)	DC (Volts)	Peak (Volts)	Peak (Volts)	Ave (RMS Volts)	
4000	50	3.2	.25	.033	.02	.22	.09	.026	10
	260	2.2	.22	.022	.01	.15	.08	.024	
	500	2.2	.25	.018	.01	.11	.05	.015	
	740	1.2	.10	.012	.00	.07	.02	.007	
	970	1.0	.06	.008	.00	.04	.01	.002	
5000	50	4.2	.34	.048	.05	.27	.12	.034	10
	260	3.4	.32	.037	.04	.21	.11	.034	
	500	1.7	.26	.035	.04	.18	.10	.030	
	740	1.9	.21	.030	.03	.15	.08	.024	

TABLE I. ENDURANCE RIG TEST DATA,
STANDARD-RACE FAULTED BEARING, S/N 3

Speed RPM	Thrust Load (Lbs)	Accel. Raw Signal (Volts)	Filtered Signal at 25 KH_z		Envelope Detected Signal		Filtered Envelope Signal at Inner-Race Ball-Pass Freq.		Charge Amplifier Setting (MV/G)
			Peak (Volts)	Ave (RMS Volts)	DC (Volts)	Peak (Volts)	Peak (Volts)	Ave (RMS Volts)	
4000	50	.20	.038	.012	.005	.032	.006	.006	10
	260	.18	.020	.007	.005	.011	.004	.003	
	500	.16	.020	.007	.005	.011	.004	.003	
	740	.16	.022	.007	.008	.016	.005	.004	
	970								
5000	50	.29	.038	.014	.005	.028	.005	.005	10
	260	.27	.031	.011	.000	.018	.004	.004	
	500	.24	.023	.009	.000	.014	.004	.004	
	740	.22	.024	.009	.000	.014	.004	.004	

TABLE II. ENDURANCE RIG TEST DATA
STANDARD-RACE USED BEARING, S/N 4

Speed RPM	Thrust Load (Lbs)	Accel. Raw Signal (Volts)	Filtered Signal at 25 KH_z		Envelope Detected Signal		Filtered Envelope Signal at Inner-Race Ball-Pass Freq.		Charge Amplifier Setting (MV/G)
			Peak (Volts)	Ave (RMS Volts)	DC (Volts)	Peak (Volts)	Peak (Volts)	Ave (RMS Volts)	
4000	50	.14	.023	.007	.02	.017	.004	.0004	10
	260	.10	.016	.005	.02	.013	.004	.0003	
	500	.10	.020	.006	.02	.016	.005	.0004	
	740	.10	.024	.007	.02	.018	.005	.0005	
	970	.08	.025	.006	.00	.020	.006	.0007	
5000	50	.26	.090	.021	.01	.090	.010	.0002	10
	260	.16	.020	.007	.01	.013	.004	.0003	
	500	.14	.023	.007	.01	.017	.004	.0004	
	740	.14	.026	.008	.01	.020	.004	.0004	

TABLE III ENDURANCE RIG TEST DATA
STANDARD-RACE USED BEARING SN 9
(2300 hours, noisy)

Speed RPM	Thrust Load (Lbs)	Accel. Raw Signal (Volts)	Filtered Signal at 25 KHz		Envelope Detected Signal		Filtered Envelope Signal at Inner-Race Ball-Pass Freq.		Charge Amplifier Setting (MV/G)
			Peak (Volts)	Ave (RMS Volts)	DC (Volts)	Peak (Volts)	Peak (Volts)	Ave (RMS Volts)	
4000	50	.13	.035	.008	.01	.032	.005	.0006	10
	260	.11	.013	.004	.01	.007	.004	.0003	
	500	.10	.015	.004	.01	.010	.004	.0002	
	740	.10	.020	.005	.01	.014	.004	.0003	
	970	.10	.018	.005	.01	.014	.004	.0003	
5000	50	.19	.062	.015	.01	.045	.009	.0010	10
	260	.17	.030	.008	.00	.022	.006	.0007	
	500	.16	.035	.009	.00	.026	.005	.0005	
	740	.14	.036	.009	.00	.030	.005	.0005	

TABLE IV. ENDURANCE RIG TEST DATA
STANDARD-RACE USED BEARING SN 10
(2300 hours, noisy)

Speed RPM	Thrust Load (Lbs)	Accel. Raw Signal (Volts)	Filtered Signal at 15 KH_z		Envelope Detected Signal		Filtered Envelope Signal at Inner-Race Ball-Pass Freq.		Charge Amplifier Setting (MV/G)
			Peak (Volts)	Ave (RMS Volts)	DC (Volts)	Peak (Volts)	Peak (Volts)	Ave (RMS Volts)	
4000	50	1.8	.13	.024	.02	.13	.03	.005	100
	260	1.8	.14	.025	.02	.14	.03	.006	
	500	1.6	.18	.034	.03	.17	.04	.009	
	740	1.7	.18	.033	.03	.18	.035	.008	
	970	2.0	.20	.040	.05	.30	.03	.004	
5000	50	2.9	.35	.055	.06	.34	.04	.007	100
	260	2.1	.31	.057	.07	.28	.05	.011	
	500	2.5	.40	.060	.09	.34	.07	.020	
	740	2.8	.33	.058	.07	.30	.06	.016	

TABLE V. ENDURANCE RIG TEST DATA
HEAVY RACE, FAULTED BEARING, S/N 3
(Signal at 15 KH_z)

Speed RPM	Thrust Load (lbs)	Accel. Raw Signal (Volts)	Filtered Signal at 15 KH_z		Envelope Detected Signal		Filtered Envelope Signal at Inner-Race Ball-Pass Freq.		Charge Amplifier Setting (MV/G)
			Peak (Volts)	Ave (RMS Volts)	DC (Volts)	Peak (Volts)	Peak (Volts)	Ave (RMS Volts)	
4000	50	.32	.05	.009	.01	.06	.006	.0006	100
	260	.31	.05	.009	.01	.06	.006	.0007	
	500	.28	.05	.009	.01	.05	.006	.0007	
	740	.32	.04	.007	.02	.04	.005	.0005	
	970	.28	.03	.005	.02	.04	.004	.0004	
5000	50	.43	.06	.012	.01	.06	.006	.0006	100
	260	.38	.06	.011	.01	.06	.006	.0010	
	500	.37	.07	.015	.01	.07	.008	.0010	
	740	.35	.06	.009	.01	.06	.008	.0010	

TABLE VI. ENDURANCE RIG TEST DATA
HEAVY RACE, USED BEARING, S/N 4
(Signal at 15 KH_z)

Speed RPM	Thrust Load (Lbs)	Accel. Raw Signal (Volts)	Filtered Signal			Envelope Detected Signal		Filtered Envelope Signal at Inner Race Ball-Pass Freq.		Charge Amplifier Setting (MV/G)
			KH_z	Peak (Volts)	Ave (RMS Volts)	DC (Volts)	Peak (Volts)	Peak (Volts)	Ave (RMS Volts)	
4000	50	1.8	37	.40	.07	.08	.64	.11	.026	100
	260	1.8	46	.26	.10	.03	.54	.07	.012	
	500	1.6	52	.18	.08	.08	.29	.03	.004	
	740	1.7	57	.16	.07	.08	.36	.07	.016	
	970	2.0	58	.23	.09	.12	.53	.15	.037	
5000	50	2.9	36	.68	.20	.27	1.40	.23	.045	100
	260	2.1	46	.29	.13	.17	.60	.08	.012	
	500	2.5	52	.40	.15	.19	.70	.12	.022	
	740	2.8	54	.39	.16	.21	.80	.20	.044	

TABLE VII. ENDURANCE RIG TEST DATA
HEAVY RACE, FAULTED BEARING, S/N 3
(Load-Dependent High Frequency Response)

Speed RPM	Thrust Load (Lbs)	Accel. Raw Signal (Volts)	Filtered Signal			Envelope Detected Signal		Filtered Envelope Signal at Inner Race Ball-Pass Freq.		Charge Amplifier Setting (MV/G)
			KH_z	Peak (Volts)	Ave (RMS Volts)	DC (Volts)	Peak (Volts)	Peak (Volts)	Ave (RMS Volts)	
4000	50	.32	37	.11	.036	.03	.17	.015	.0027	100
	260	.31	46	.10	.045	.03	.20	.024	.0045	
	500	.28	52	.07	.037	.02	.15	.015	.0030	
	740	.32	54	.11	.054	.04	.24	.030	.0065	
	970	.28	56	.10	.050	.04	.22	.028	.0060	
5000	50	.43	35	.22	.079	.08	.35	.040	.0067	100
	260	.38	45	.14	.060	.06	.25	.035	.0062	
	500	.37	50	.15	.074	.07	.30	.038	.0067	
	740	.35	53	.11	.059	.05	.24	.030	.0050	

TABLE VIII. ENDURANCE RIG TEST DATA
HEAVY RACE, USED BEARING, S/N 4
(Load-Dependent High Frequency Response)

Brg. Ident.	Test Rig	Raw Signal Peak (Volts)	Filtered Signal KH_z	Filtered Signal Peak (Volts)	Filtered Signal Ave (RMS Volts)	Envelope Detected Signal DC (Volts)	Envelope Detected Signal Peak (Volts)	Filtered Envelope At Inner-Race Ball-Pass Freq. (580 H_z) Peak (Volts)	Filtered Envelope At Inner-Race Ball-Pass Freq. (580 H_z) Ave (RMS Volts)
SN 3 Faulted	ENDU	1.05	41	.45	.077	.10	.40	.10	.010
	LTF Side #1	.84	35	.55	.115	.15	.45	.13	.020
SN 4 Used	ENDU.	.64	34	.28	.061	.08	.23	.05	.007
	LTF Side #2	.06	34	.03	.007	.01	.02	.01	.001
SN 003 from Side #1 LTF	ENDU.	.96	36	.35	.073	.10	.24	.05	.006
	LTF Side #1	.32	34	.19	.041	.06	.14	.04	.005
SN 012 from Side #2 LTF	ENDU.	.45	31	.15	.022	.04	.10	.02	.002
	LTF Side #2	.12	33	.07	.012	.02	.04	.01	.001

TABLE IX. LTF DATA vs ENDURANCE-RIG DATA
AT 4000 RPM, 50 LB LOAD,
HEAVY-RACE BEARINGS

Brg. Ident.	Raw Signal Peak (Volts)	Filtered Signal			Envelope Detected Signal		Filtered Envelope Signal at Inner-Race Ball-Pass Freq. (1320 H_z)		Charge Amp Setting (MV/G)
		Resonance Freq. KH_z	Peak (Volts)	Ave (RMS Volts)	DC (Volts)	Peak (Volts)	Peak (Volts)	Ave (RMS Volts)	
SN 3 Faulted	1.35	31	.51	.165	.250	.60	.150	.022	100
SN 4 Used	.45	31	.15	.048	.066	.17	.046	.006	
SN 003 from LTF Side #1	.73	34	.25	.090	.125	.30	.085	.012	
SN 012 from LTF Side #2	.24	37	.06	.022	.033	.07	.018	.002	

TABLE X. LTF DATA AT 9100 RPM, HEAVY RACE BEARINGS

LIST OF FIGURES

LIST OF FIGURES
(continued)

Figure

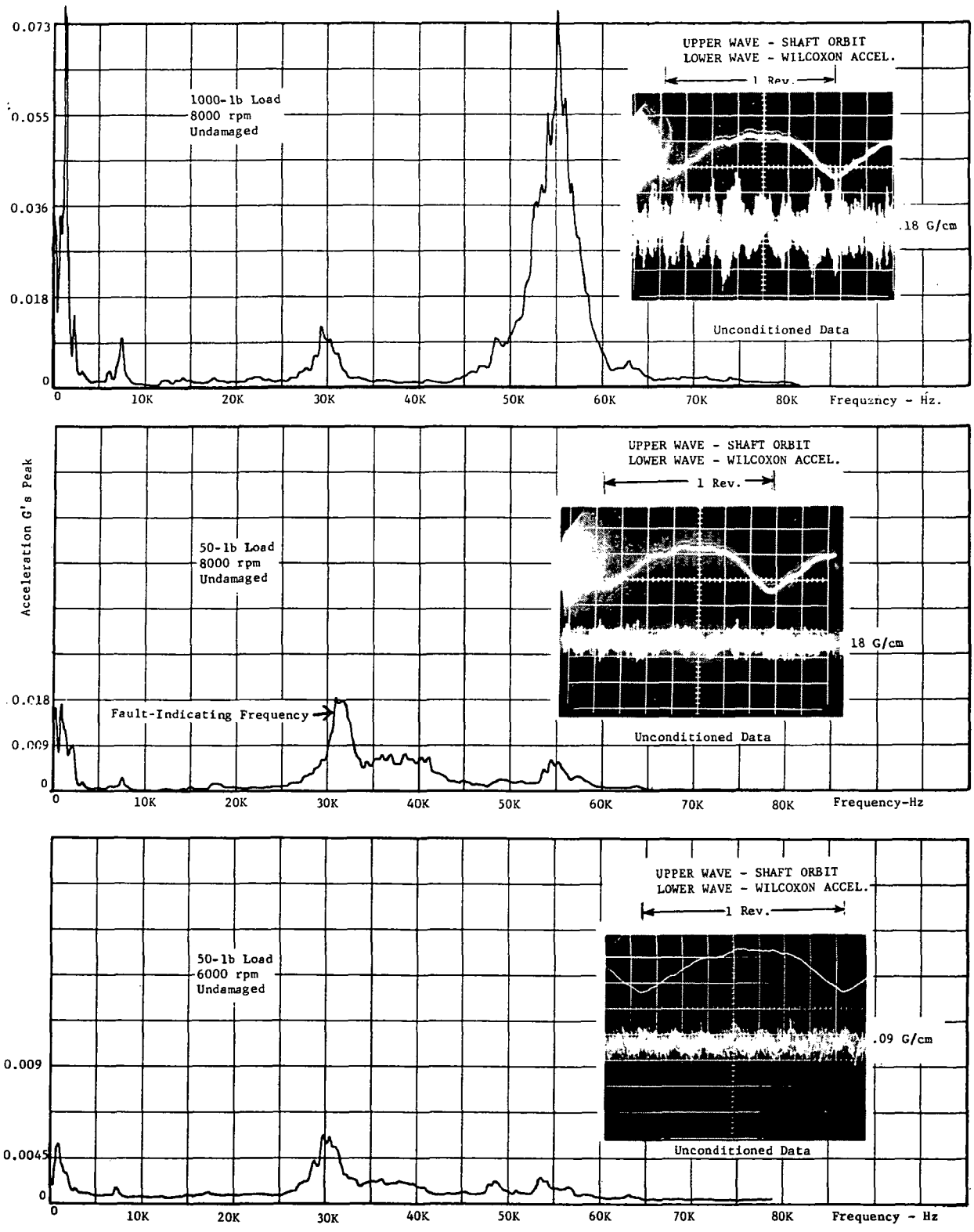

Figure 1 Illustration of Constant Fault-Indicating Frequency in Undamaged Bearing when Load and Speed were Varied

FOLDOUT FRAME

FOLDOUT FRAME

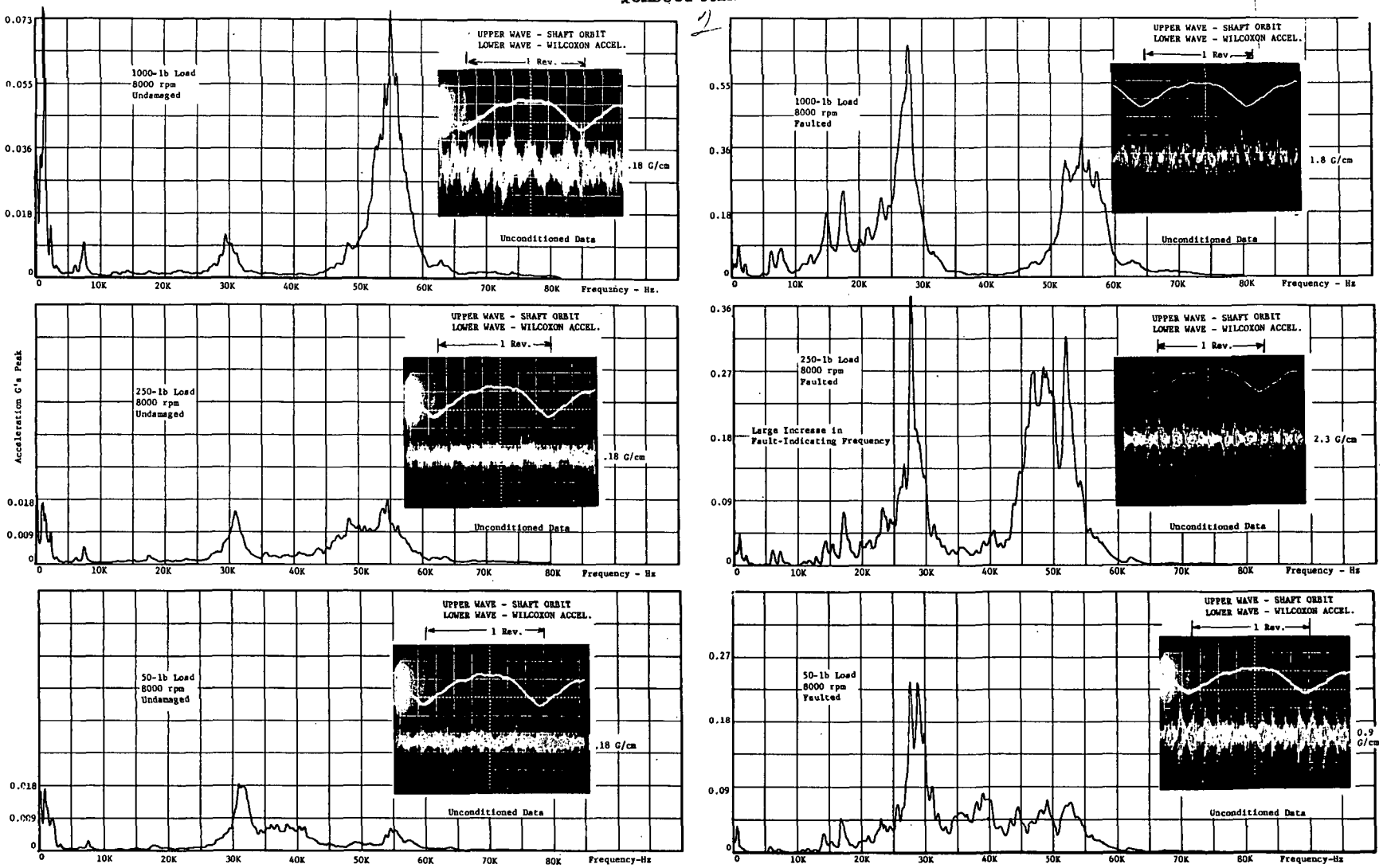

Figure 2 Illustrating Amplitude Increase of Fault-Indicating Frequency for Faulted Bearing

42

MTI-15560

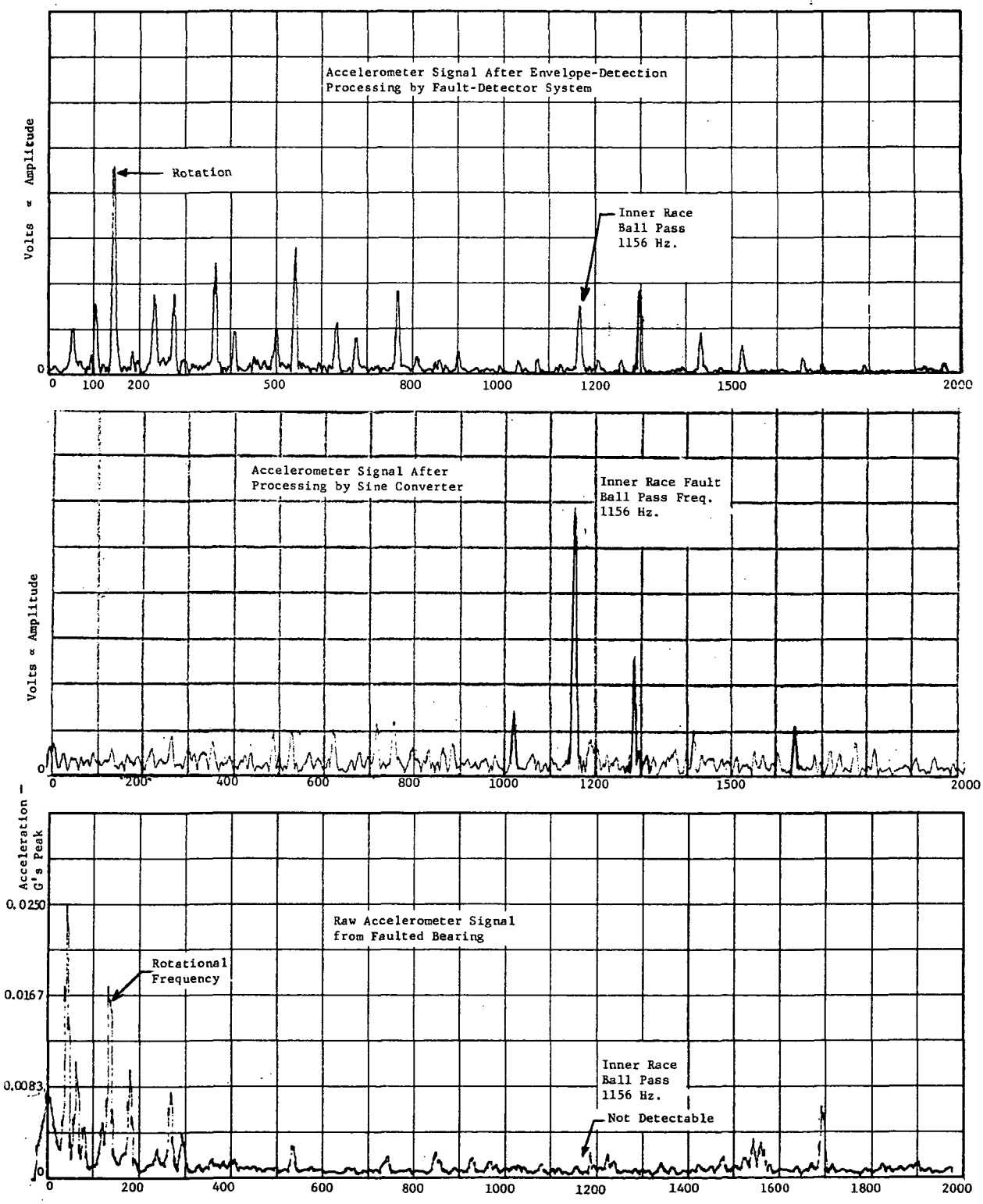

Figure 3 Illustrating Absence of Ball-Passing Frequency in Raw Signal and Need for Envelope Detection

MTI-15562

This page is reproduced at the back of the report by a different reproduction method to provide better detail.

Figure 4 Bearing Fault Detector

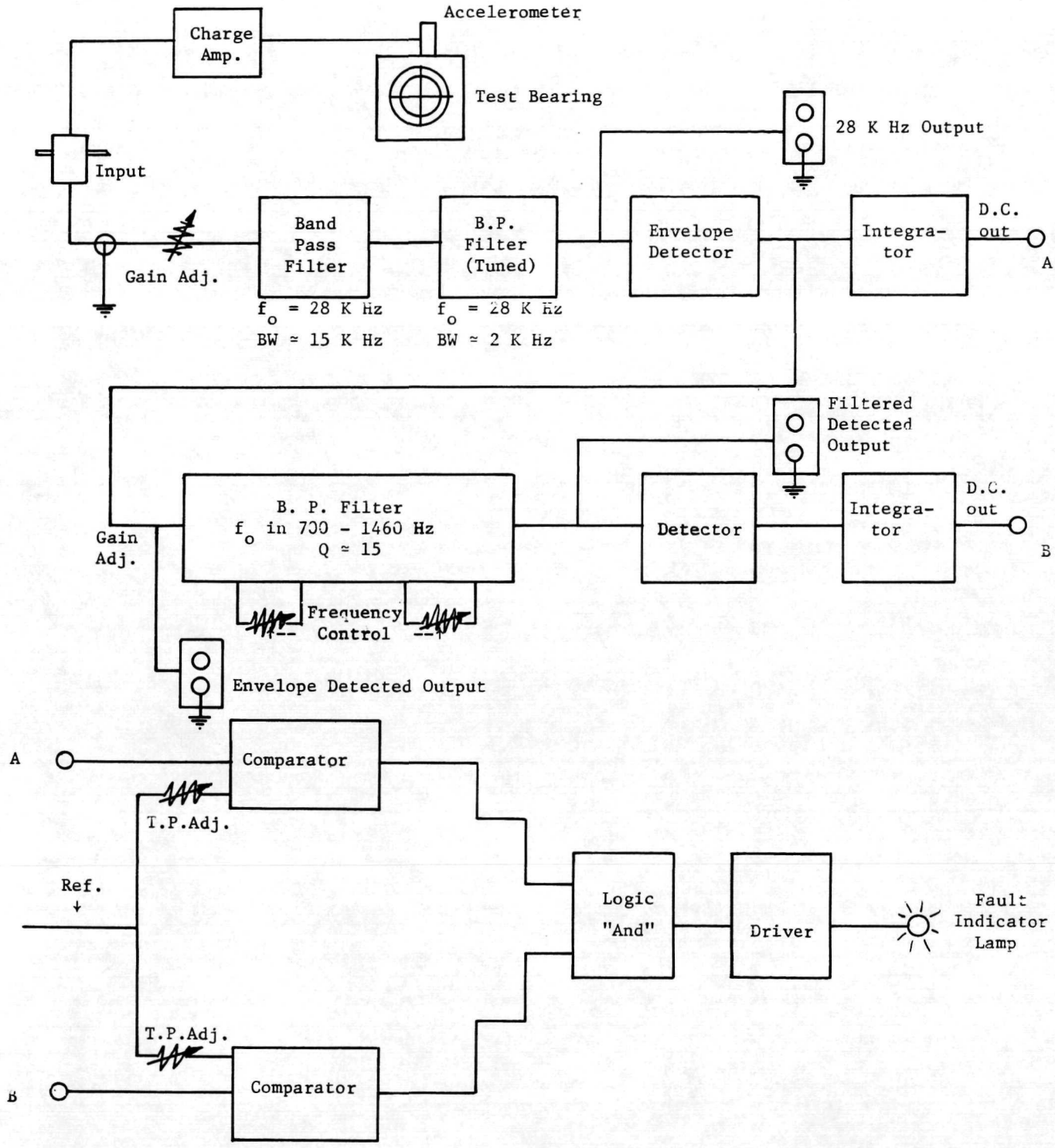

Figure 5 Schematic of Bearing Fault Detector

MTI-12118

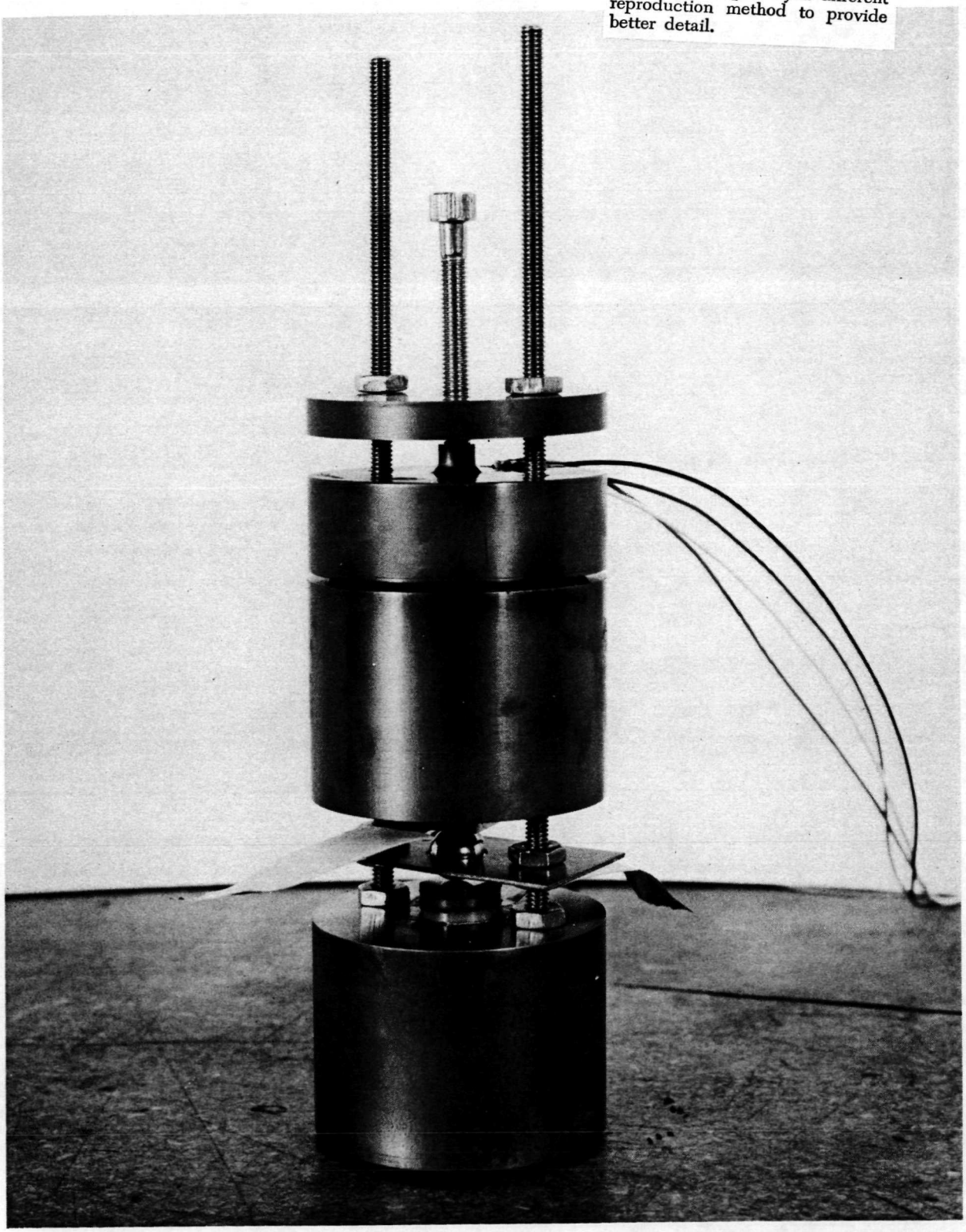

Figure 6 Ball Resonance Test Fixture, Assembled

MTI-12863

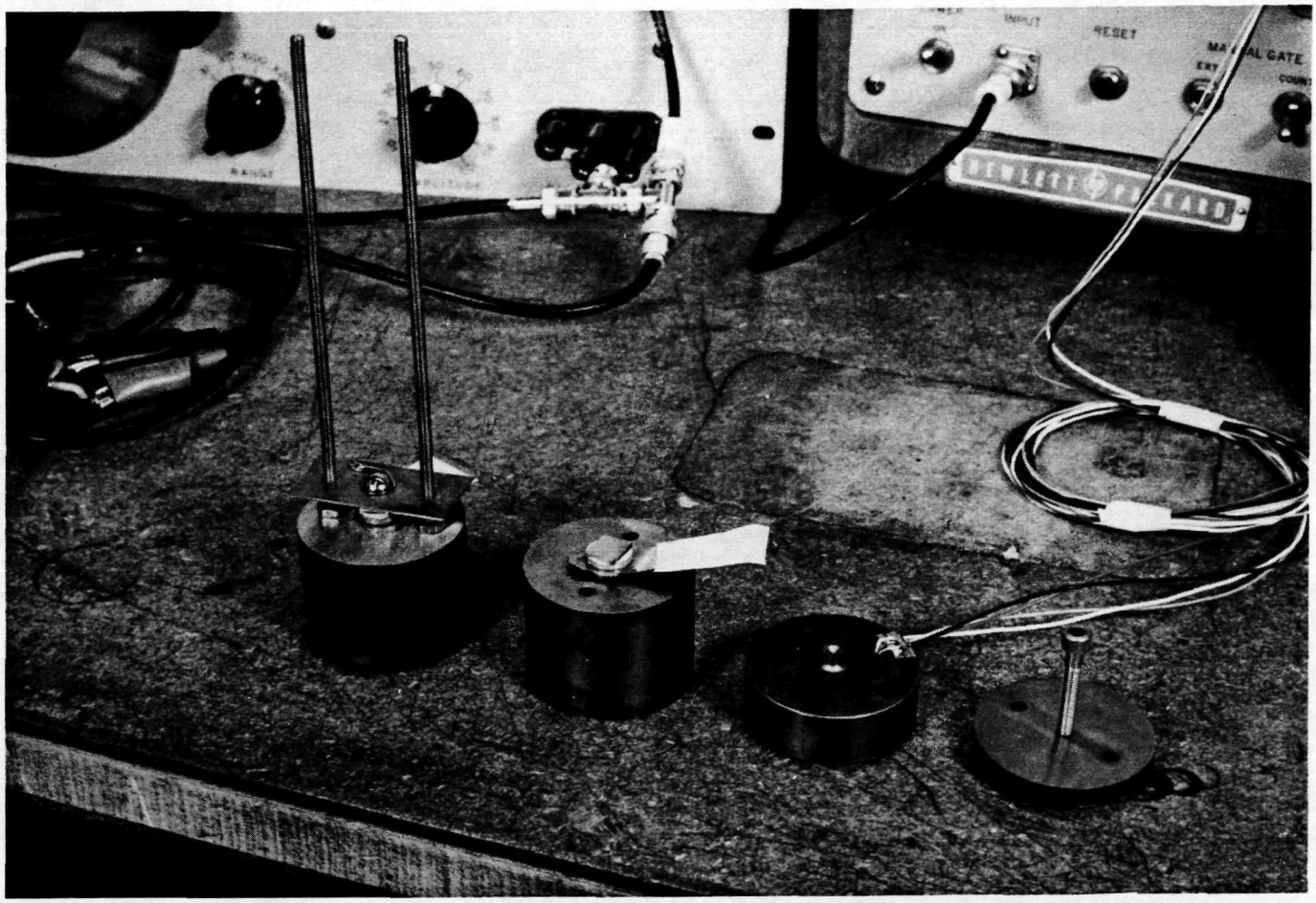

This page is reproduced at the back of the report by a different reproduction method to provide better detail.

Figure 7 Ball Resonance Test Fixture, Disassembled

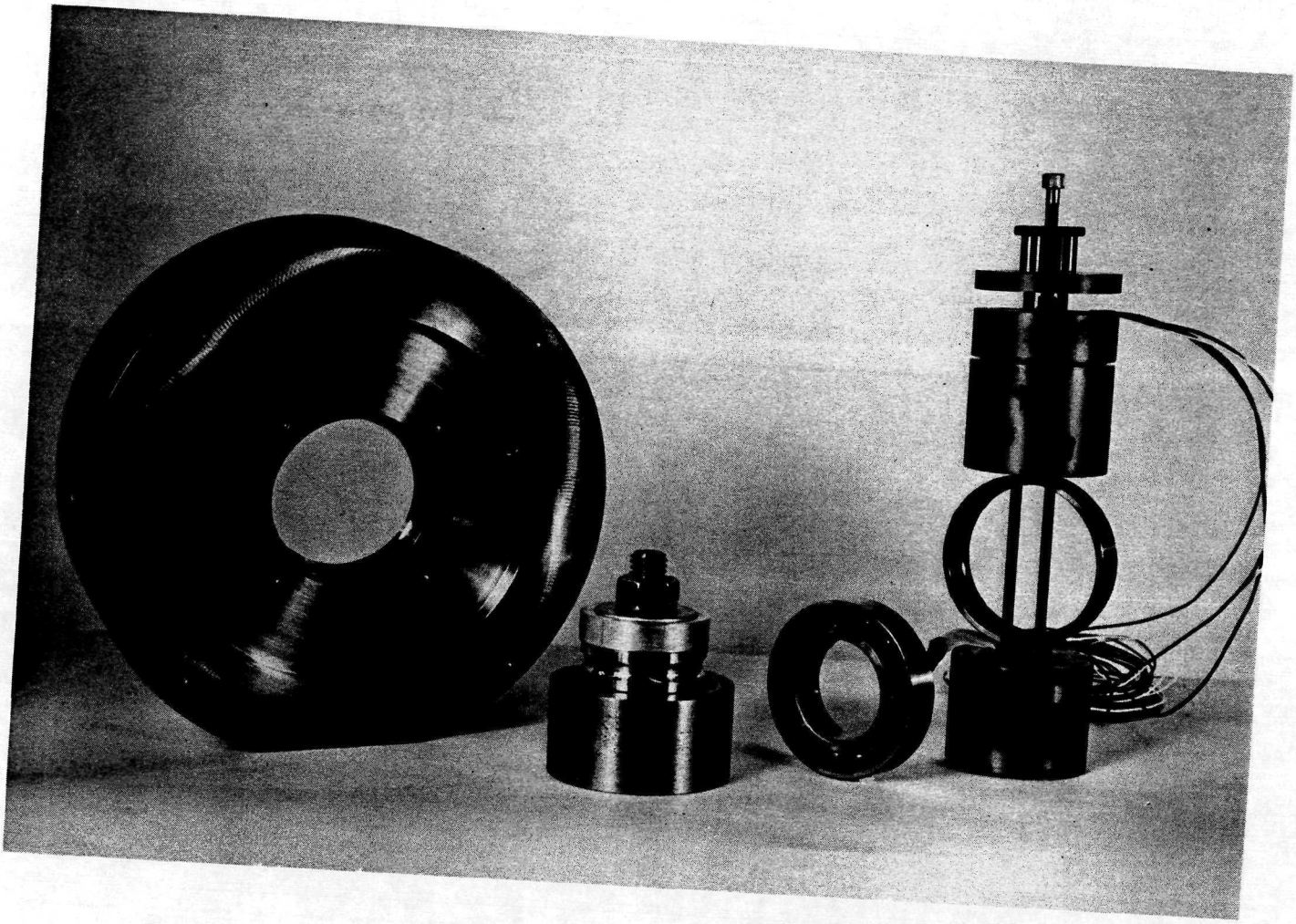

This page is reproduced at the back of the report by a different reproduction method to provide better detail.

Figure 8 Shown Here from Left to Right are:

Outer Race of Type 107H Ball Bearing Mounted in NASA Program Fixture
Inner Race of Type 107H Ball Bearing Mounted in NASA Program Fixture
Complete Type 107H Bearing
Outer Race of Type 107H Bearing Mounted in Ball Resonance Test Fixture

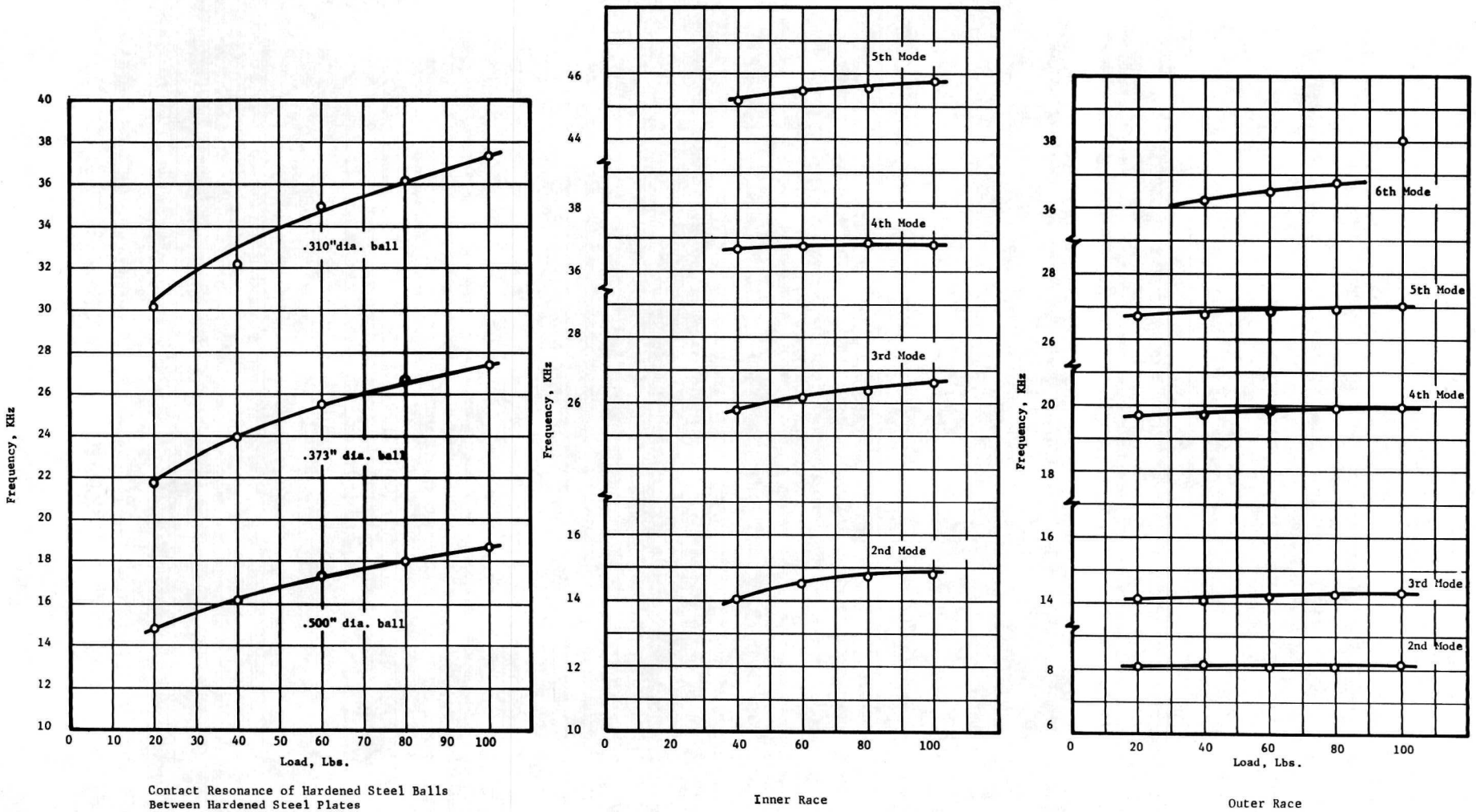

Figure 9 Variation of Resonant Frequencies with Load for Components of Type 107H Ball Bearing, Tested in Ball Contact Resonance Test Fixture

MTI-15586

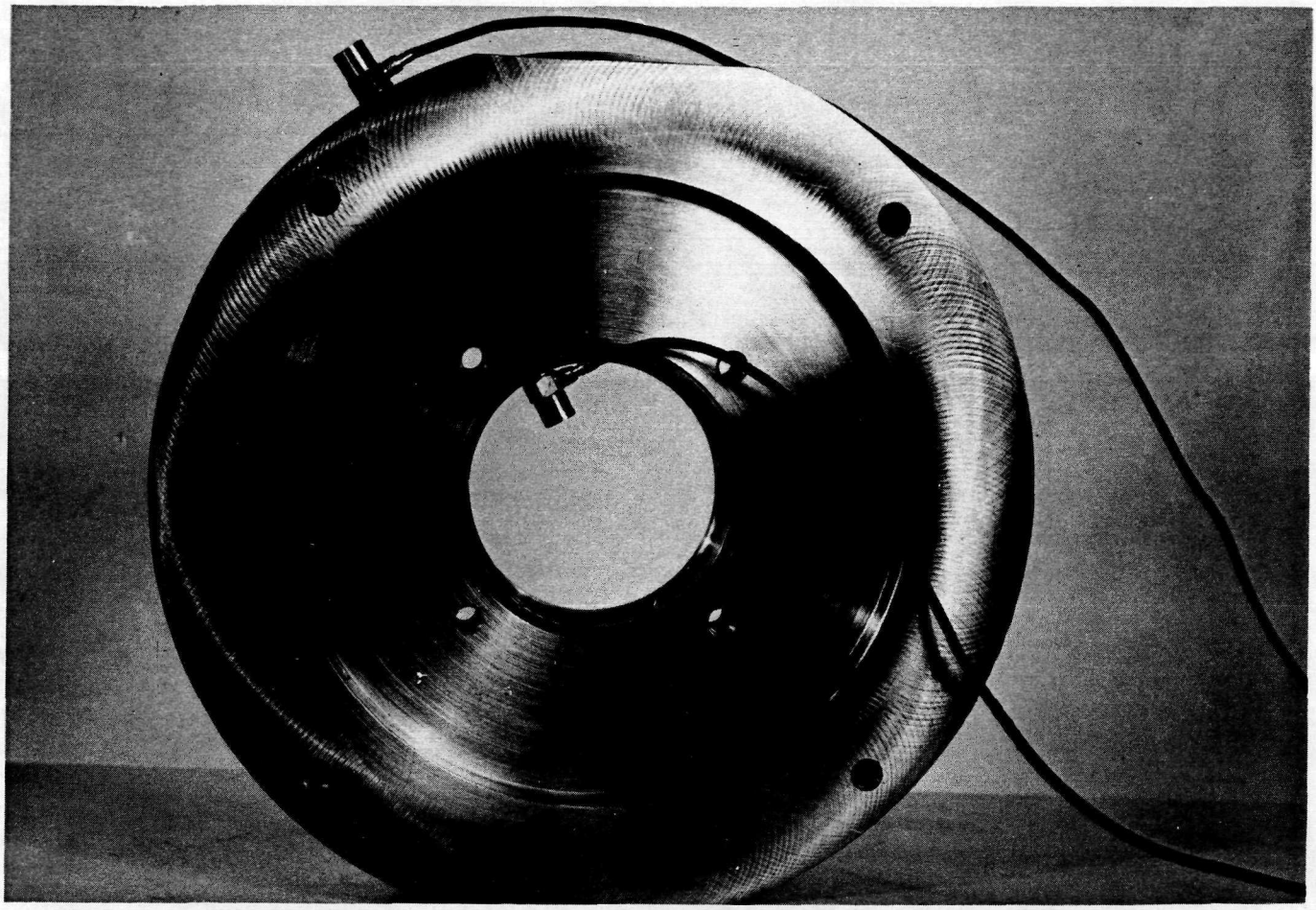

This page is reproduced at the back of the report by a different reproduction method to provide better detail.

Figure 10 Outer Race of Type 107H Bearing Mounted in NASA Program Fixture, Showing Location of "Driver" Accelerometer on I.D. of Outer Race and Pickup Accelerometer on O.D. of Holding Fixture

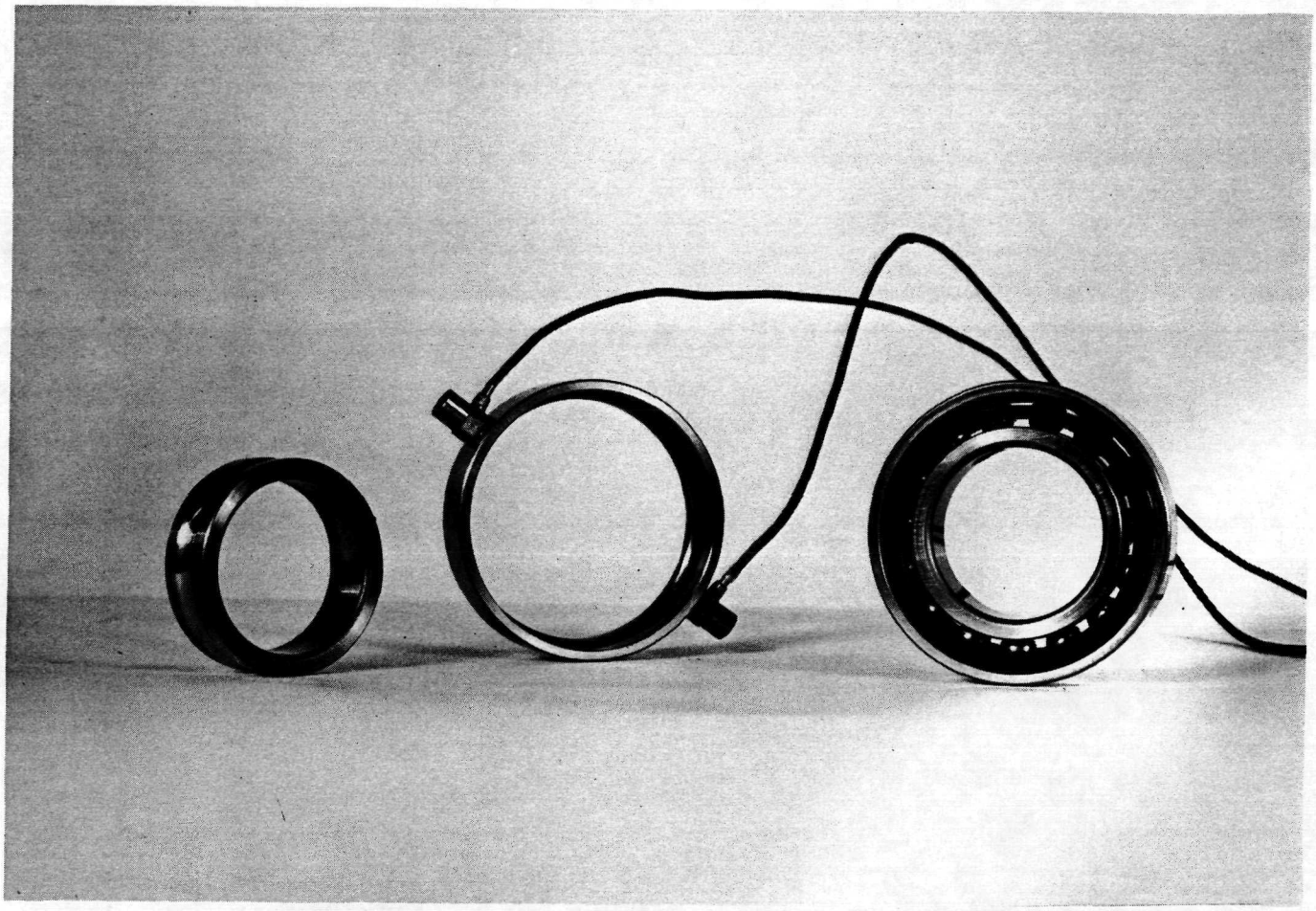

This page is reproduced at the back of the report by a different reproduction method to provide better detail.

Figure 11 Shown Here from Left to Right are:

Inner Race of Type 107H Bearing
Outer Race of Type 107H Bearing with Driver and Pichup Accelerometers
Assembled Type 107H Bearing

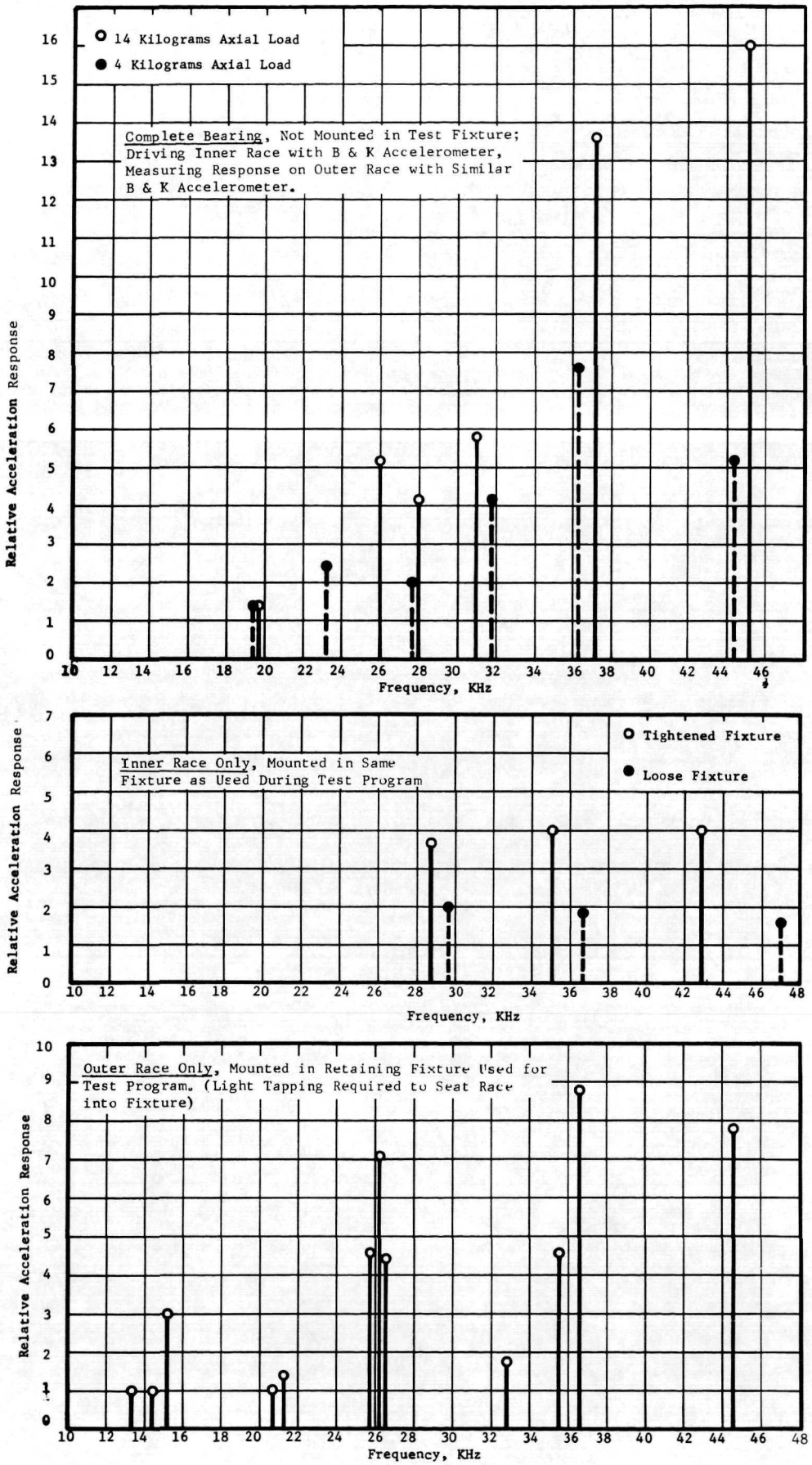

Figure 12 Relative Amplitude of Resonances of Type 107H Ball Bearing

MTI-15585

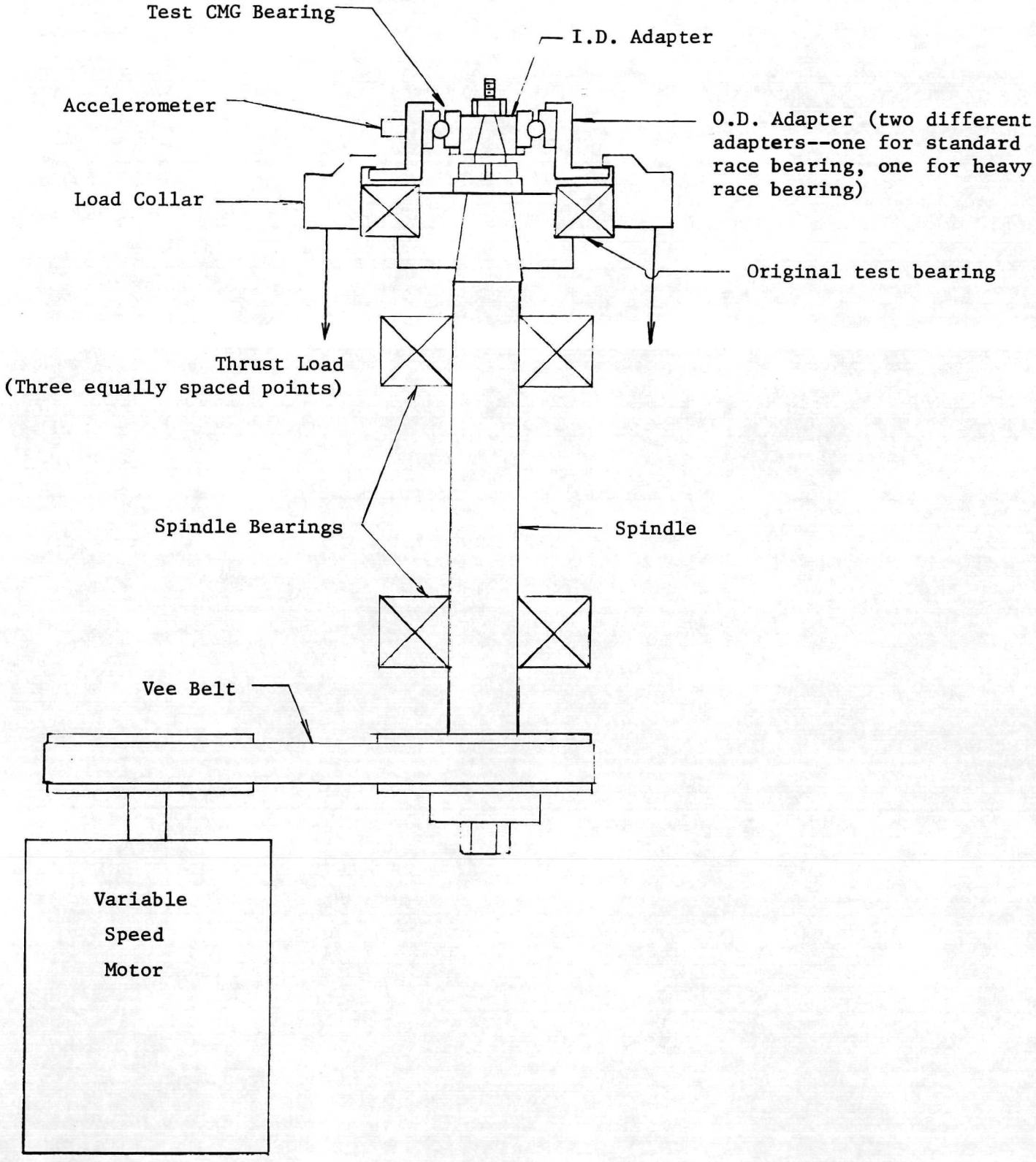

Figure 13 Modified Test Bearing Installation

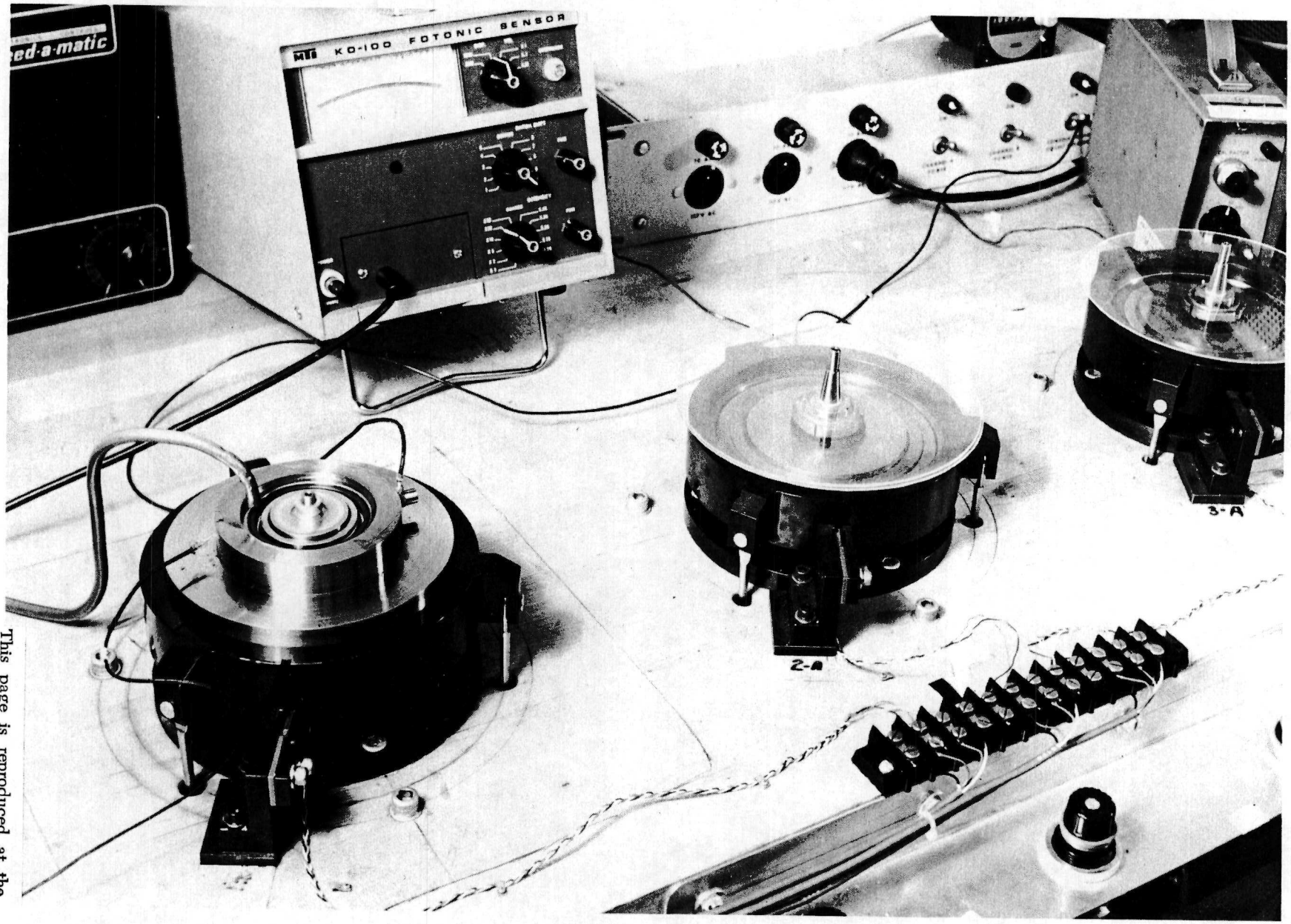

Figure 14 Standard-Race Bearing in Endurance Test Rig (Left-Hand Spindle)

MTI-15786

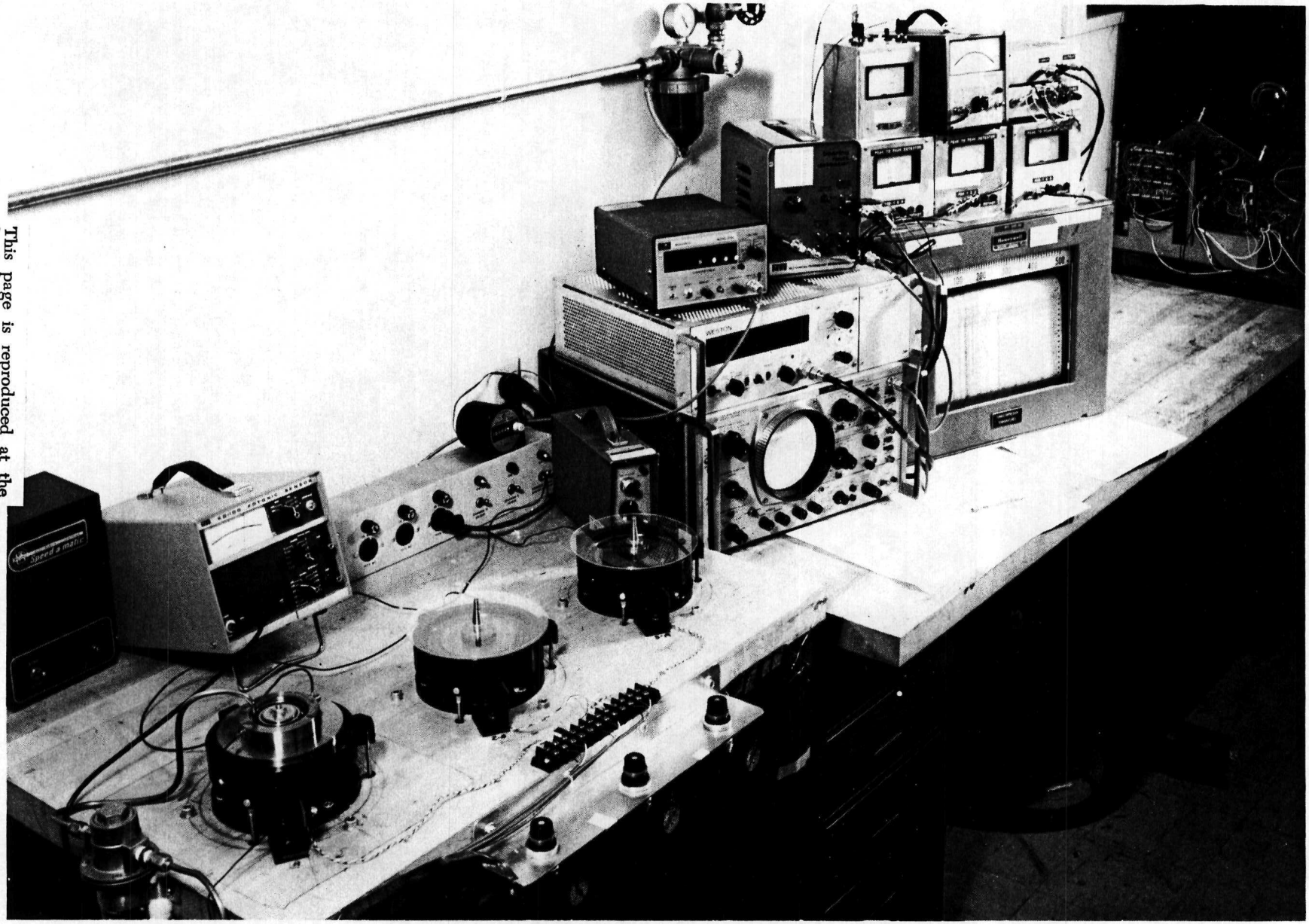

Figure 15 Endurance Rig and Instrumentation for Monitoring Test-to-Failure

MTI-15787

FOLDOUT FRAME

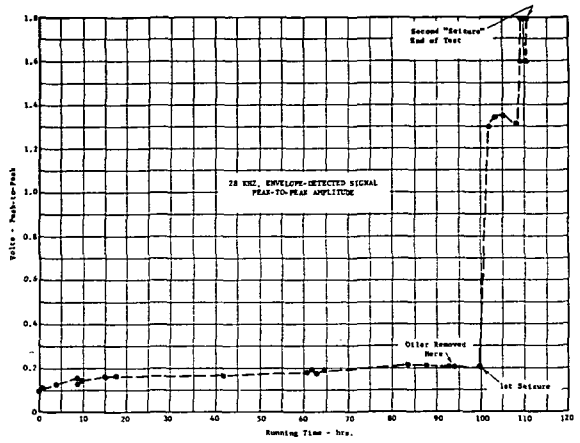

OPERATING CONDITION

4000 RPM
1100 POUNDS THRUST LOAD
OIL—MIST LUBRICATION FIRST 93 HOURS
NO OIL ADDED DURING LAST 13 HOURS
(CMG BEARING SERIAL NO.6)

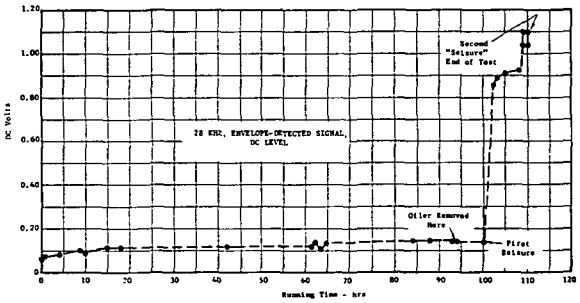

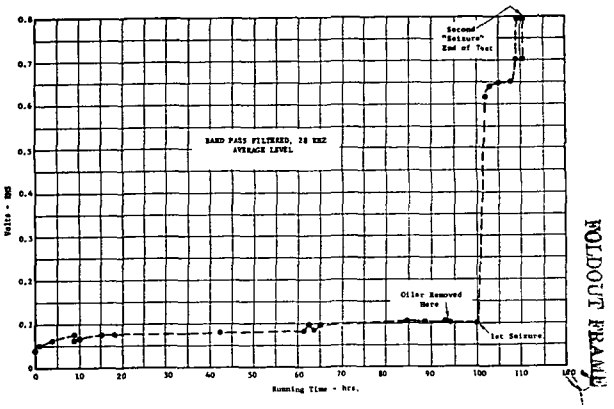

FOLDOUT FRAME

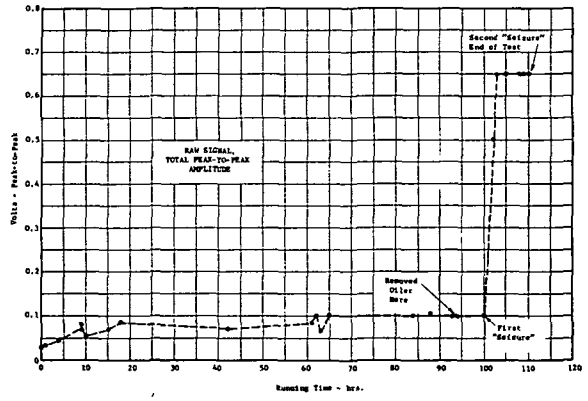

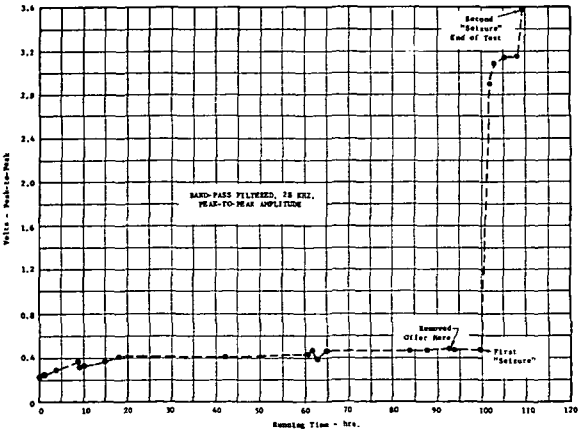

Figure 16 Time History of Accelerometer Signal During Test-to-Failure, Standard-Race 107H Bearing

96

M41-15190

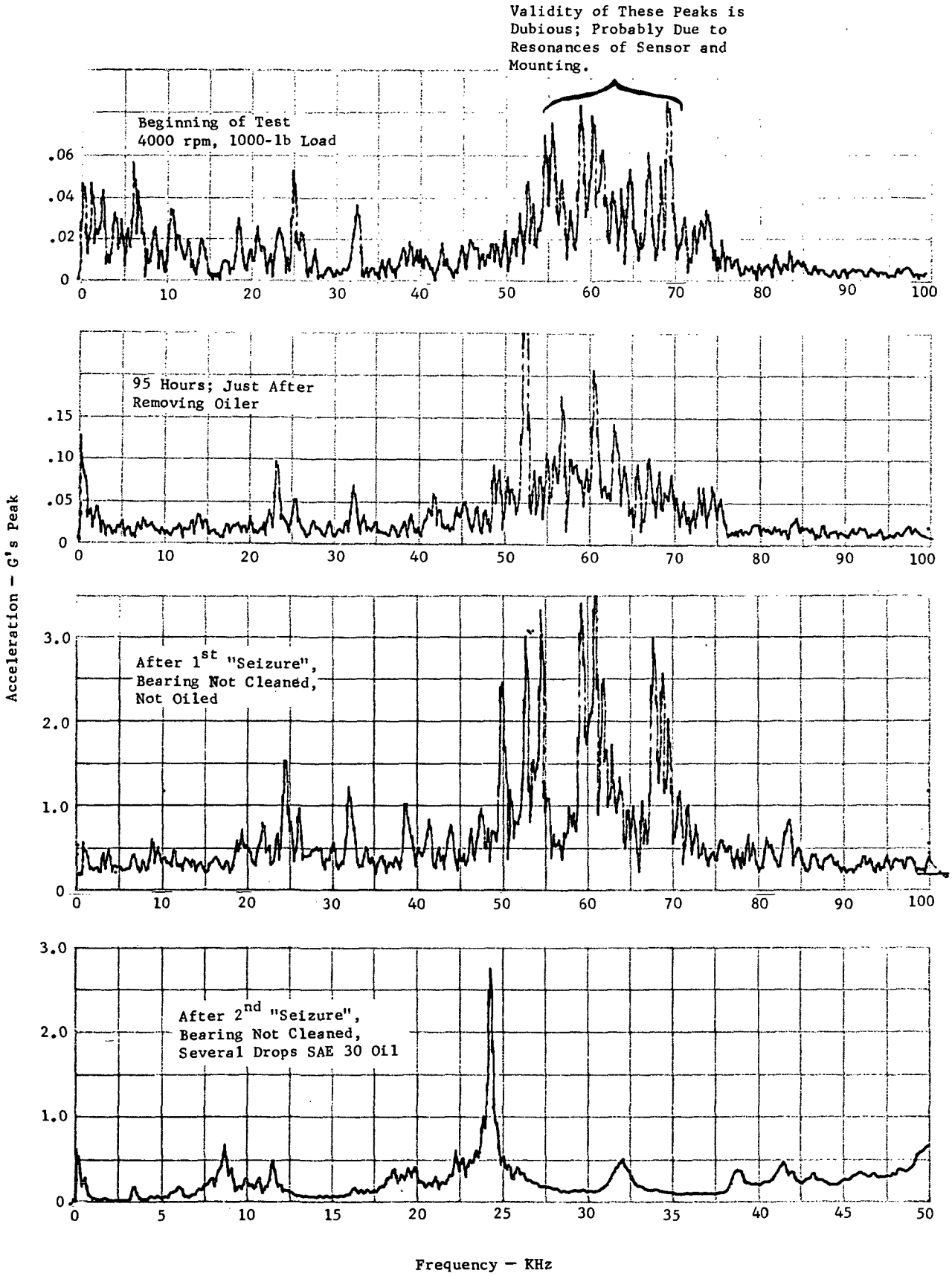

Figure 17 Frequency-Spectrum Plots of Raw Signal Taken During Test-to-Failure on Endurance Rig

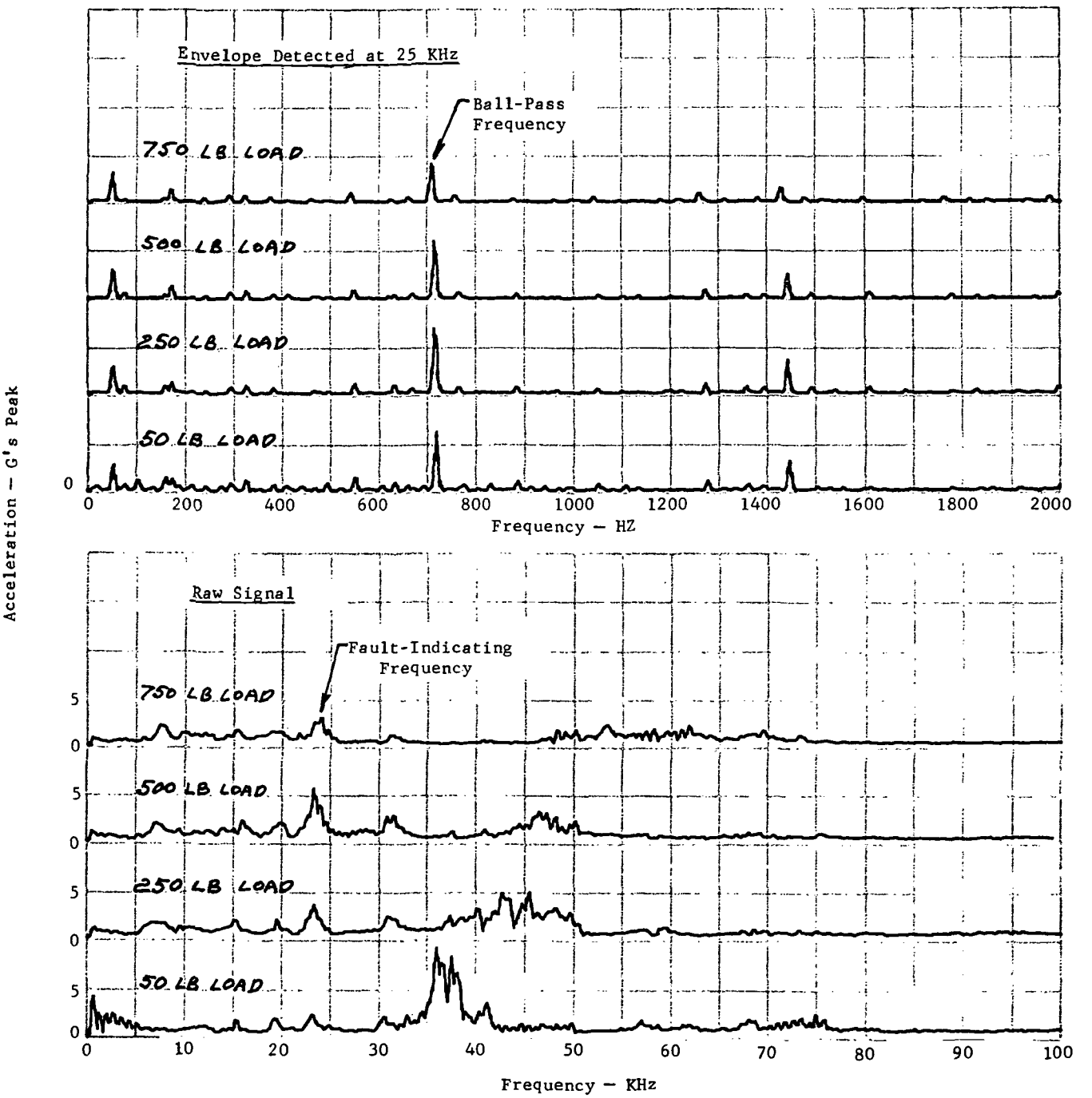

Figure 18 Frequency-Spectrum Plots for Faulted Bearing S/N 3 Tested on Endurance Rig at 5000 rpm with Various Loads

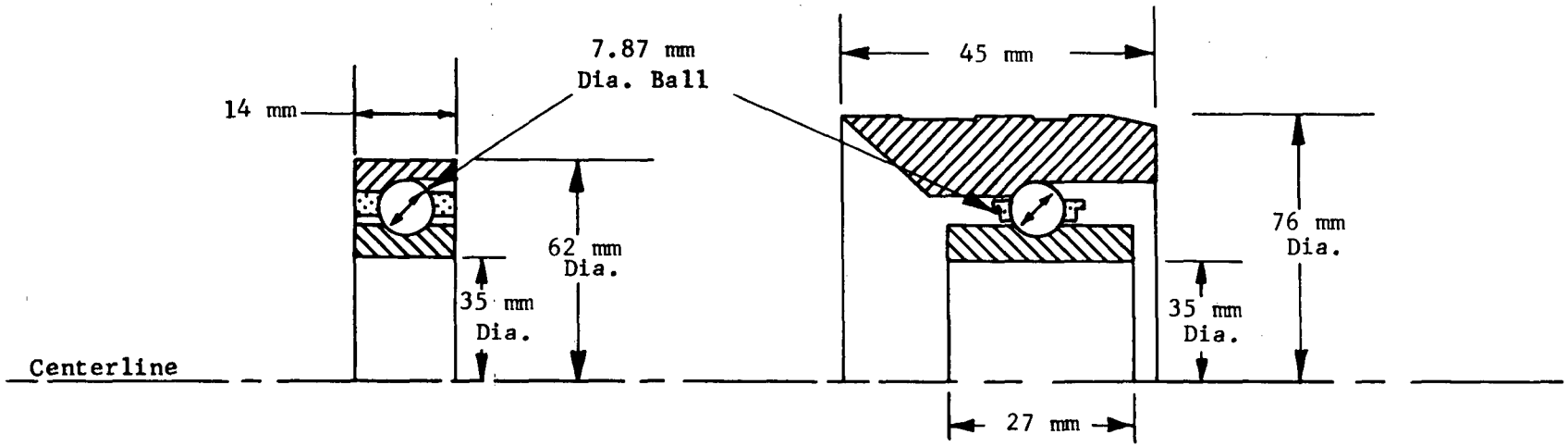

Standard Race
Barden
Part No. 107H

Heavy Race
Bendix
Part No. 2120585-F

Figure 19 Comparison of Standard and Heavy-Race 107H Bearings

MTI-15784

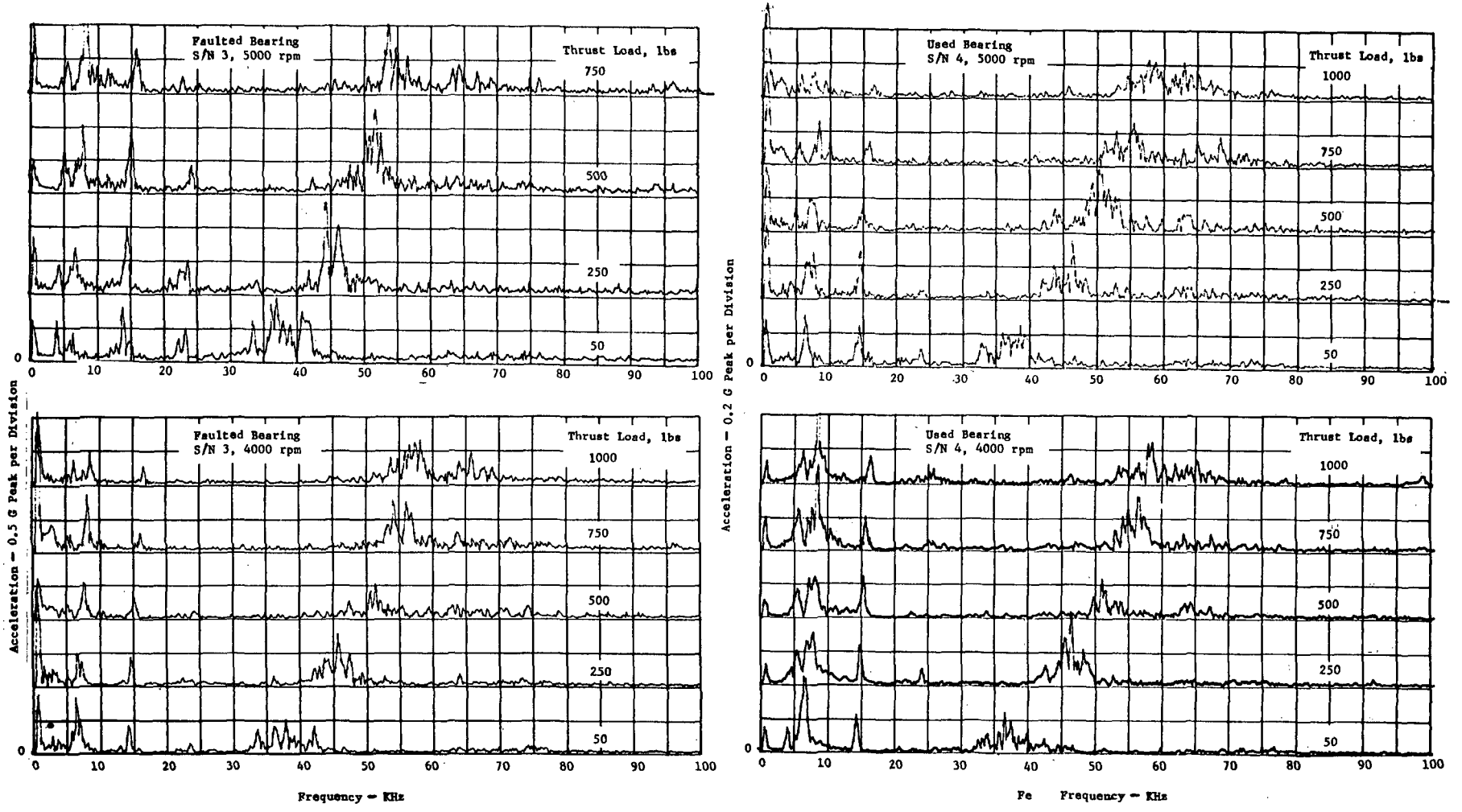

Figure 20 Frequency Spectra of Raw Signal , Heavy-Race Bearings, Endurance Test Rig

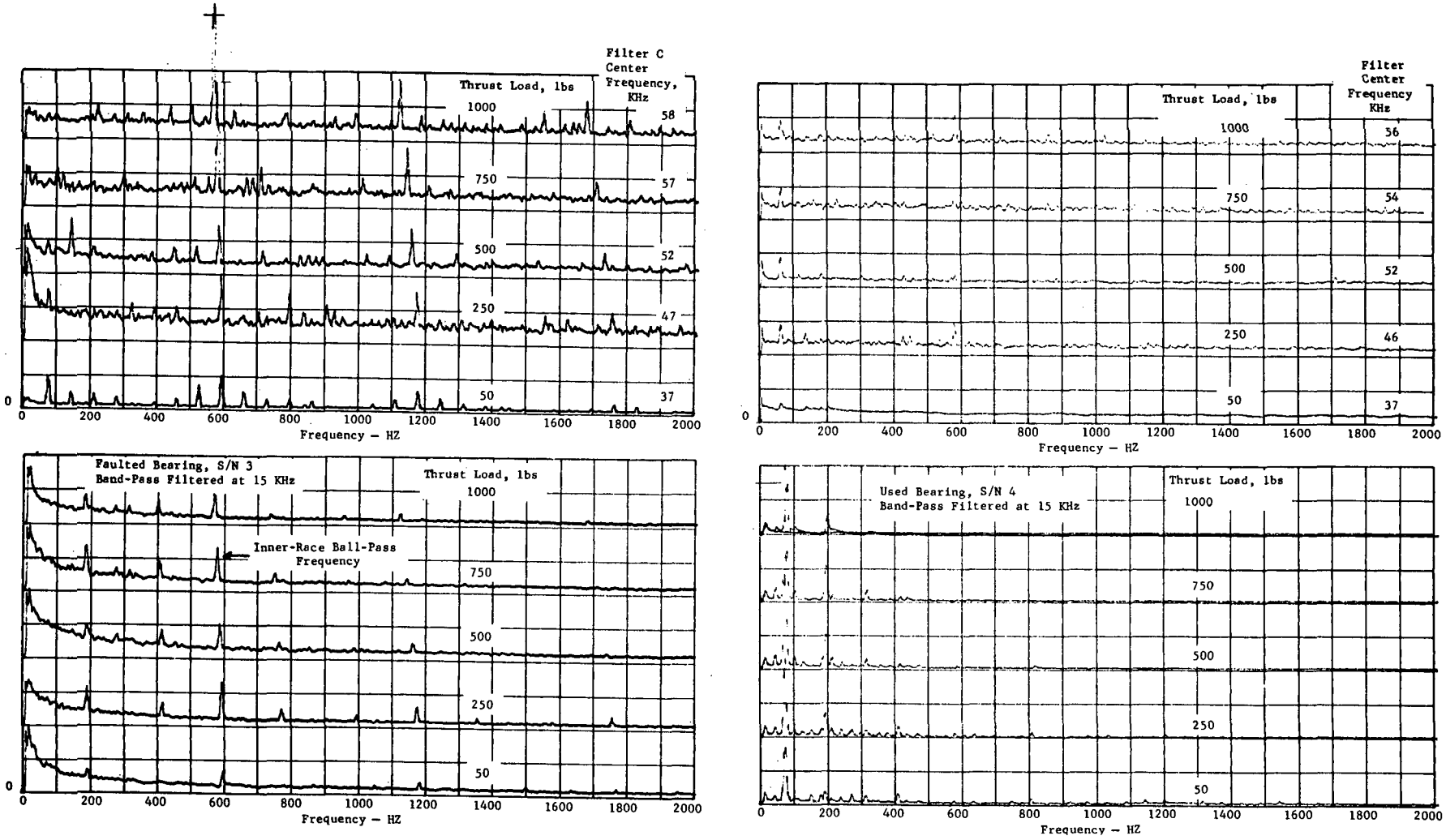

Figure 21 Frequency Spectra of Envelope-Detected Signal, Heavy-Race Bearings, Endurance Test Rig, 4000 rpm

MTI-15788

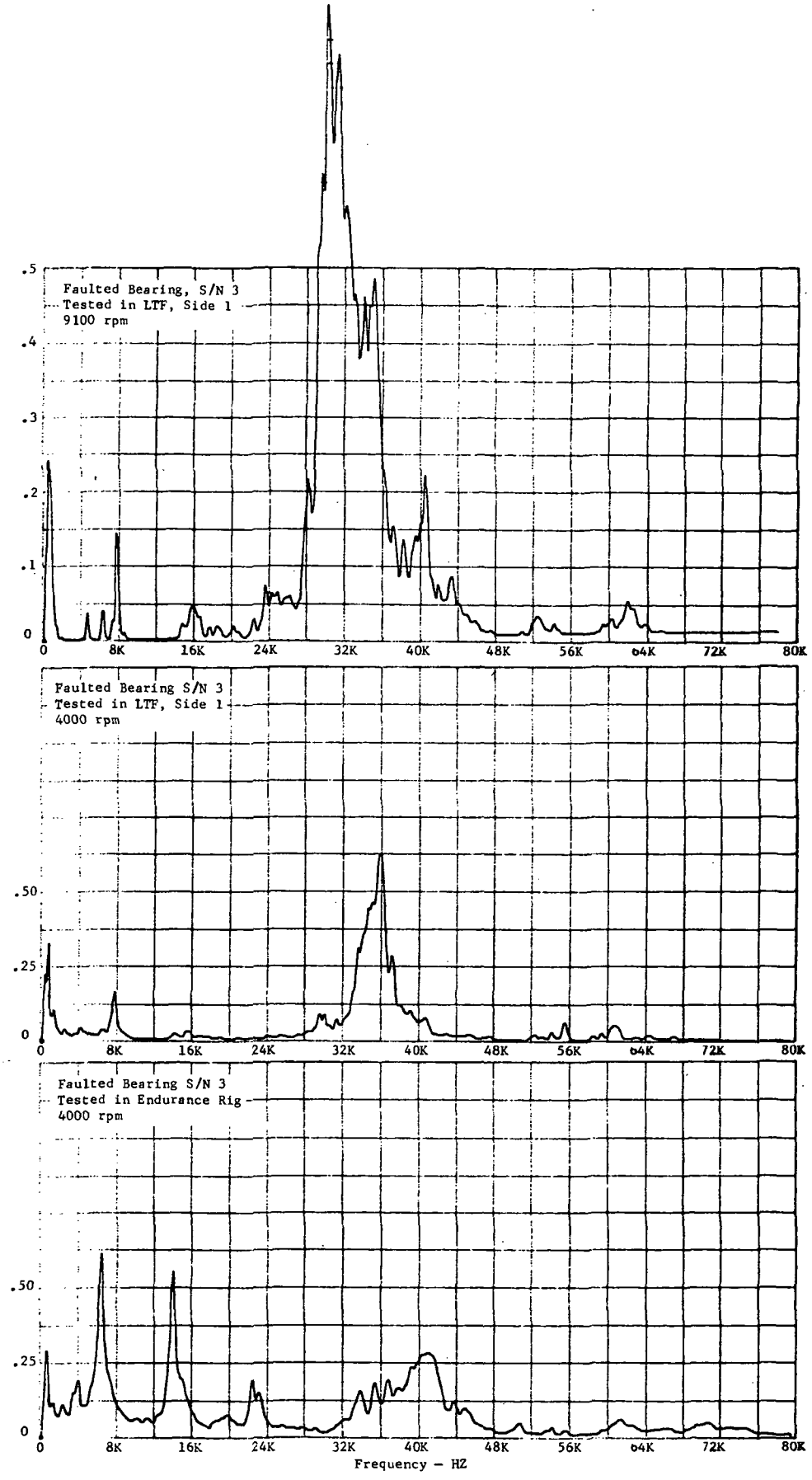

Figure 22 Comparison of Frequency Spectra from Endurance Rig and from Life Test Fixture; Faulted Bearing

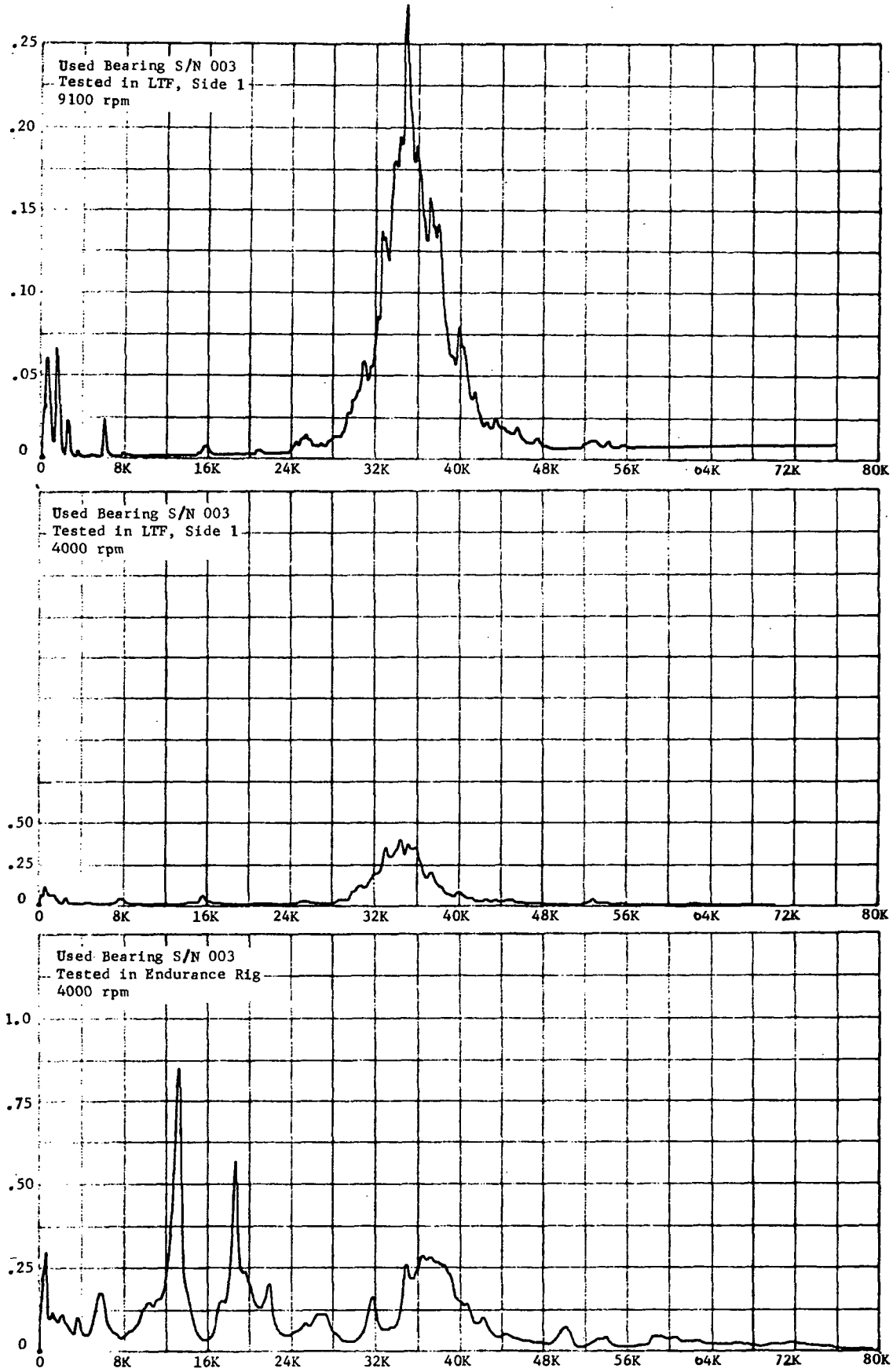

Figure 23 Comparison of Frequency Spectra from Endurance Rig and from Life Test Fixture; Used LTF Bearing

APPENDIX A

Phase I Test Spindle and Bearing

TABLE A-1

BEARING DATA:	Barden 107 H (0-9) ABEC 7
Outside diameter (62 mm)	$2.4409\ ^{-0.0002}_{+0.0000}$ inches
Bore diameter (35 mm)	$1.3780\ ^{-0.0002}_{+0.0000}$ inches
Pitch diameter	1.910 inches
Width of inner and outer race (14 mm)	$.5512\ ^{-0.001}_{+0.000}$ inches
Outer race radius of curvature	0.53 (53% of ball dia.)
Inner race radius of curvature	0.515 (51.5% of ball dia.)
Number of balls	15
Ball diameter	.3125 inches
Material (balls & races)	SAE 52100 steel
Cage material	Phenolic
Initial contact angle	$15^{o} \pm 2^{o}$ @ 10 lb. axial load
Radial Play	.0008 – .0012 inches
Value ZD^2	1.46
Static radial load rating	2640 lbs.
Static thrust load rating	7240 lbs.
Dynamic radial load rating	540 lbs. @ 8000 RPM
Basic dynamic load rating	3390 lbs.

FOLDOUT FRAME

FOLDOUT FRAME

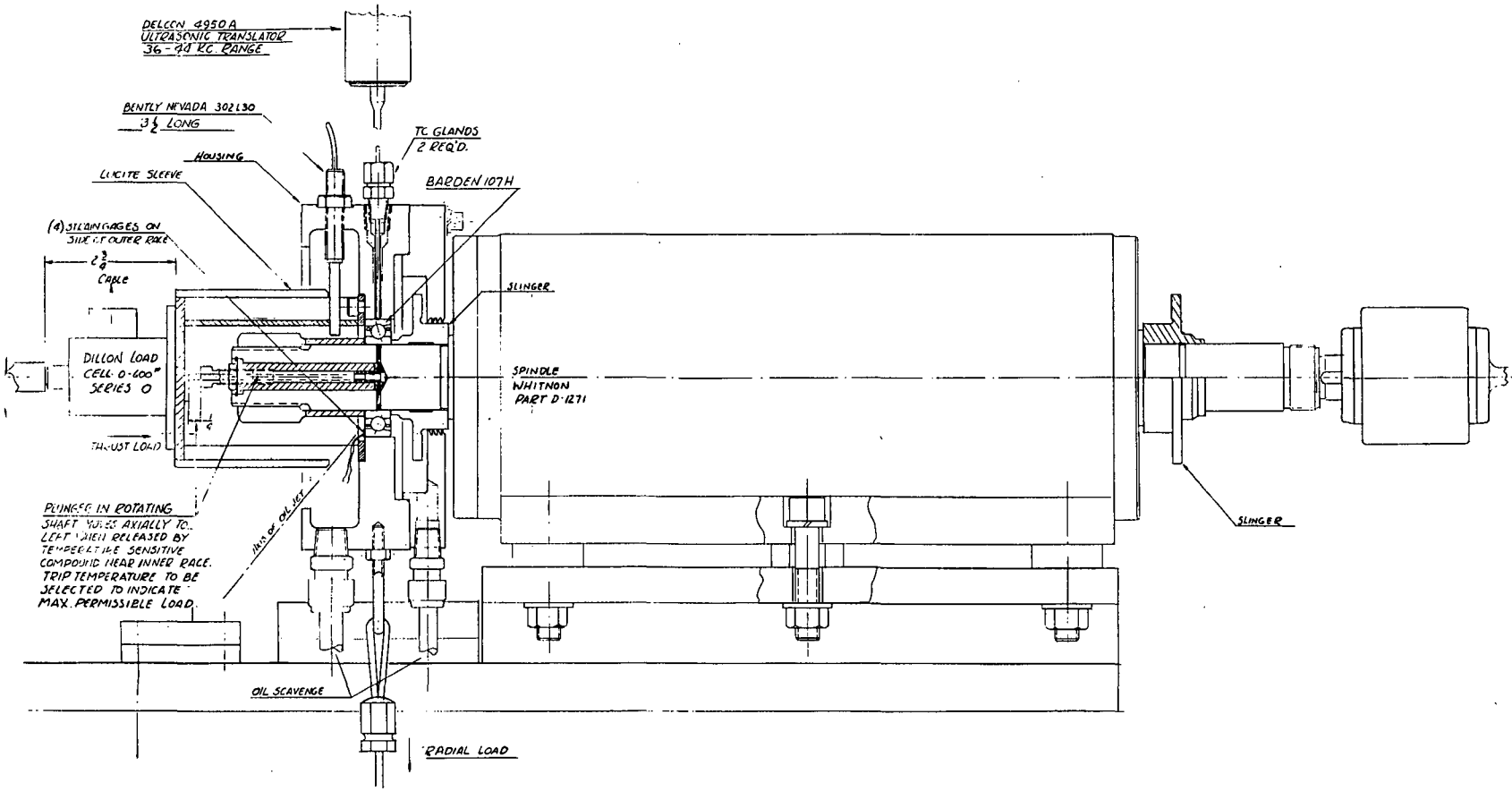

Fig. A-2 Test Bearing Spindle Assembly

MTI-12126

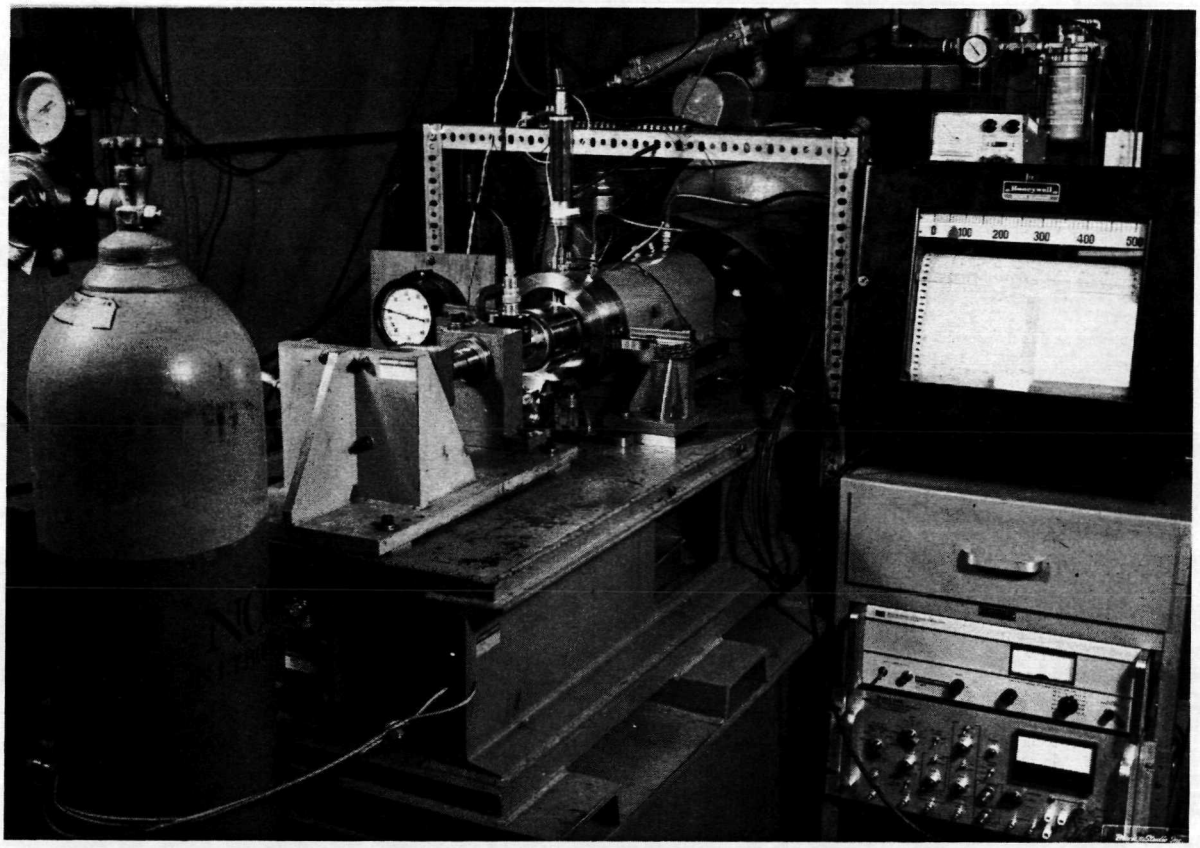

Ball Bearing Test Stand with NASA Test Bearing and Instrumentation - Cell 62

This page is reproduced at the back of the report by a different reproduction method to provide better detail.

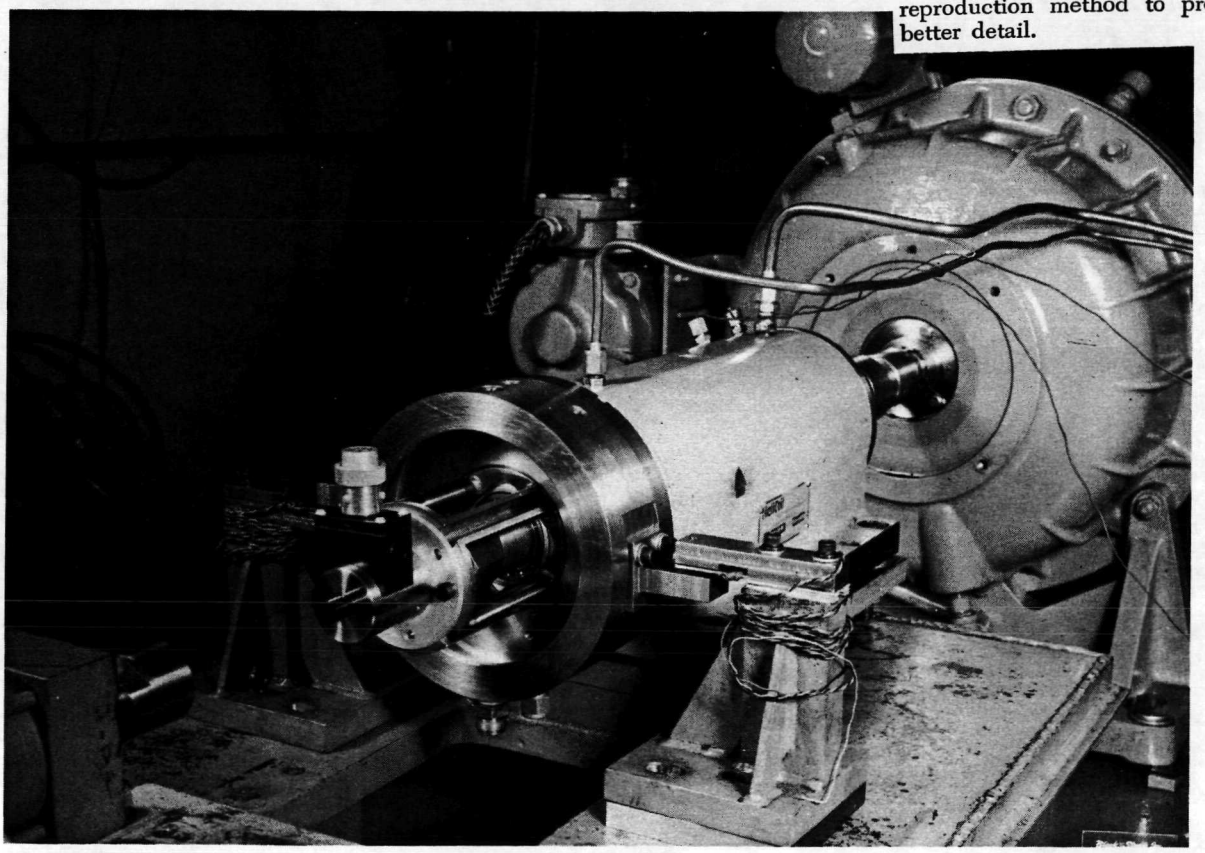

Fig. A-3 NASA Test Bearing Housing with Thrust Load Cell and Torque Arms shown

MTI-12125

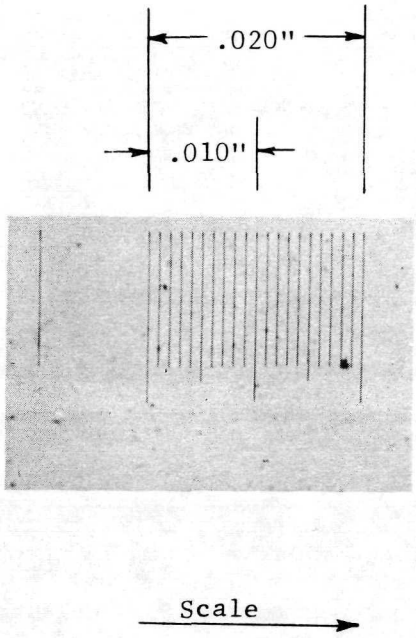

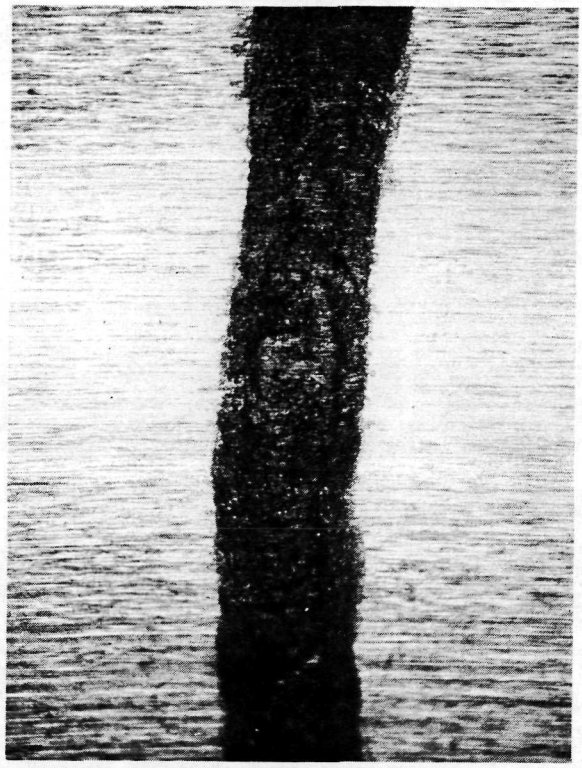

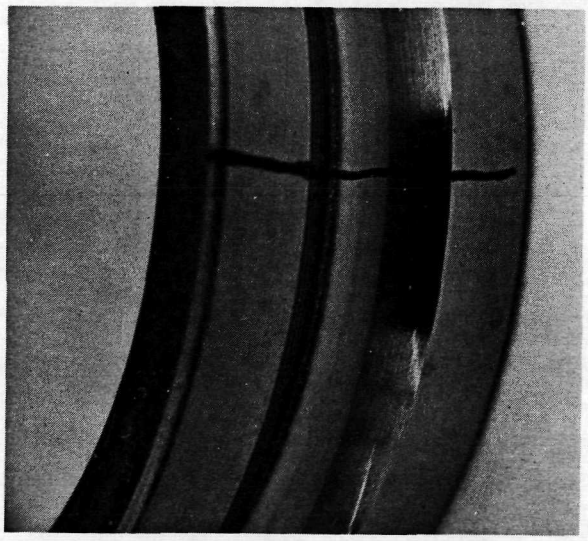

Scale 3X

This page is reproduced at the back of the report by a different reproduction method to provide better detail.

Figure A-4 Transverse Flaw Acid-Etched Across Raceway of Inner Race. Enlarged Detail Shows 0.012 inch wide by 0.0012 inch deep Fault.

TEST LOCATION Bench Test TAPE NO. _____ JOB _____ DATE 2/9/71

TEST CONDITIONS Fault Detector Filter Shape

INPUT:
TRANSDUCER Oscillator
CALIBRATOR 0.40 V peak-to-peak
AMPLIFIER _____
TAPE CHANNEL NO. _____ ☐FM ☐DIR

ANALYZER:
RANGE V,RMS _____
FREQUENCY HZ _____
GAIN 21.2V/0.4V = 53
TIME AVERAGE _____

RECORDER:
GAIN _____
X-UNITS 0 - 50,000 Hz
Y-UNITS 5.0 V AC/inch
BY R. F. Burchill

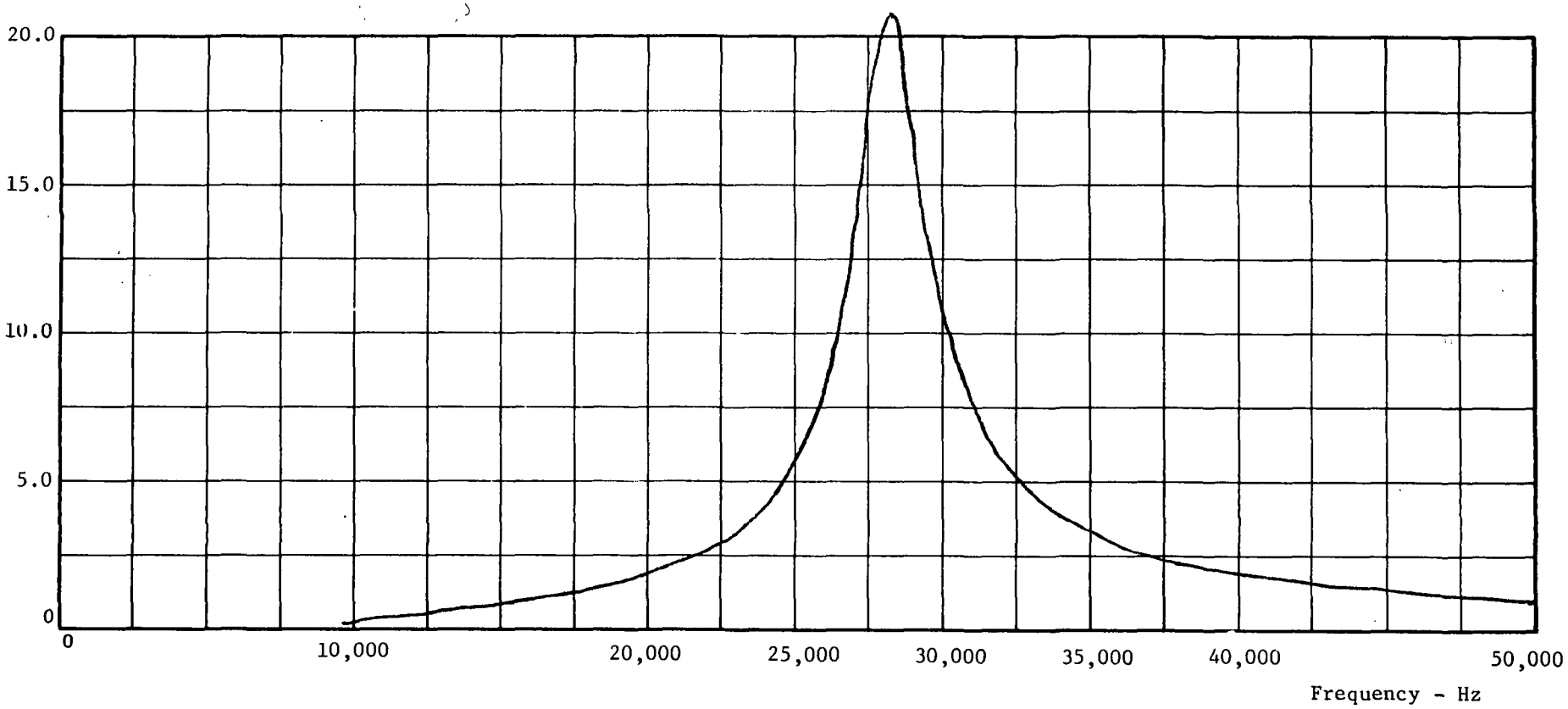

Fig. A-5 28K Hz Filter Shape, Bearing Fault Detector, Sine Wave Input Test

69

MTI-12099

APPENDIX B

Qualitative Ranking of CMG, IGRA, & LTF Units

Based upon bearing condition, unbalance levels, bearing misalignment, and acoustic noise, the overall performance ranking of CMG units is as follows:

Rank	Serial No.	Comments
Best	0008	Smooth bearings, low unbalance, low sound level, good alignment.
2	0007	As above, nearly as good as 0008
3	0009	Slightly more noisy than units above, but very good
4	0002	Bearings rough, probably due to ball wear. Unbalance fair - no mounting problems. Noise fair.
5	0010	Unit bearings good until retainer squeal - apparent mounting problems produced 2 per rev vibration. Unbalance low, noise high.
6	0004	Bearings rough, outer gimbal damaged by shake tests. Resonant response of structure to rotation frequency - even with best IG (0008).

Based upon selected parameters at 7900 rpm, ranking of IGRA units is as follows:

Rank	Serial No.	Comments
Best	E-2	Bearings fair, unbalance very good. Sound level low, bearing mounting good.
2	E-3	Bearings fair to poor, unbalance good, sound fair to poor. Bearing mounting problems present.

Both units rank below worst flight IGRA's but better overall than CMG 0010 and CMG0004.

Ranking of LTF units is as follows:

Rank	Serial No.	Comments
Best	1	Very good performance
2	4	Nearly equal
3	5	Very nearly the same - good performance
4	3	
5	2	
6	6	Bearings rough - worn - balance fair